(10)

22 July, 1997
F:1423

FEL CONSORTIUM - INTERNAL REPORT

Interpretation of Hall -Probe measurements of the wiggler

Avi Gover, Alex Arensburg, Jerzy Sokolowski, Michael Kanter

On 6/97 the wiggler magnetic field (By(z), Bz(z)) was measured along two parallel lines. The measurement data was used for the following purposes:

a. Determination of the longitudinal magnet's gradient: $\alpha = \left.\frac{dB_y}{dx}\right|_{x=0}$

b. Determination of the magnetic axis of the wiggler.

c. Computation of the magnetic field along the axis from which we deduce:

1. Best estimate for wiggler parameters (B_0).
2. Location of magnet defects.
3. Entrance and exit angles to and from the wiggler.

1. Experimental Procedure

The probe was fitted into a bore in a bronze block that could slide along the wiggler frame by means of a long screw that pulled it along the wiggler (see Figs. 1,2). The probe held two Hall - Probe sensors for axial (z) and transverse (y) magnetic field measurements. The size of the sensitive chips is 0.5 mm (?) (see Fig. 1c).

In order to measure the field gradient in the vertical (x) direction and verify our computation with redundant data, the center of the bore in the bronze block was made 0.2 mm off the physical axis of the wiggler frame in the vertical (x) dimension. After performing the first set of measurements (up), the block with the probe was rotated 180^0 around its axis and a second set of measurements (down) was carried out. The two measurements were done supposedly on two parallel lines spaced by $\delta =$ 0.4 mm (one 0.2 mm above the mechanical axis and one 0.2 mm below it). The three axes are drawn in Fig. 3 relative to the imaginary magnetic axis.

As seen from Fig. 1, the probe end was made to stick out of the bronze block 110 mm in order to be able to measure the field also out of the wiggler ends (while the block has to stay within the wiggler frame). Because of this reason we also had to interrupt the

Fig. 1

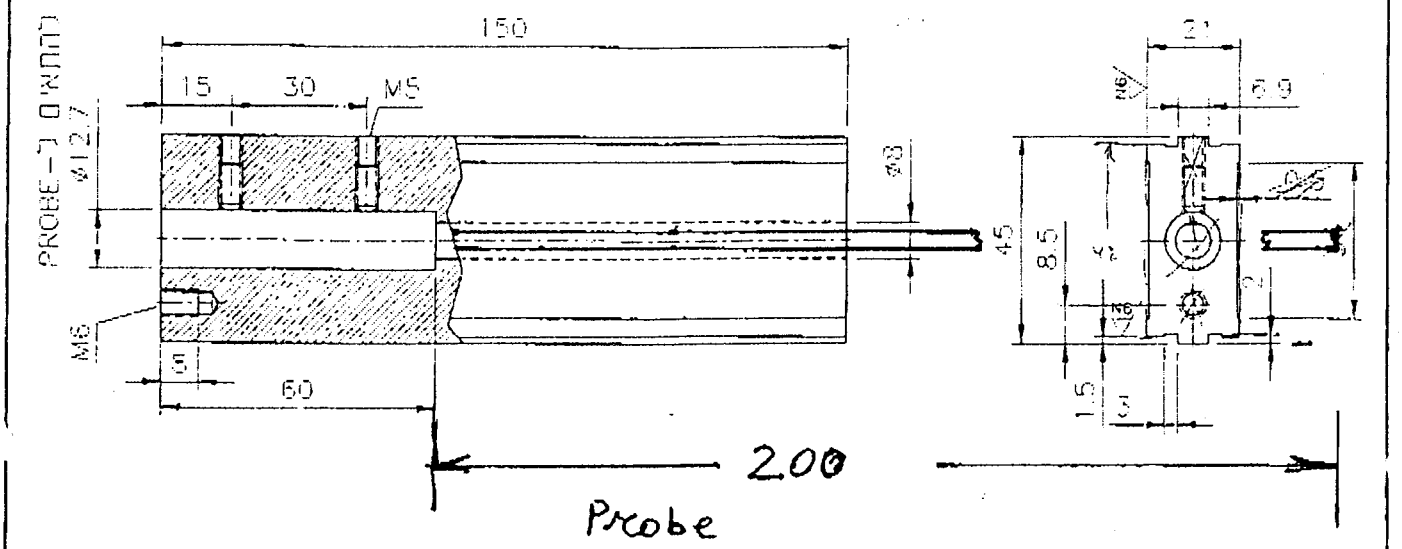

שבר פנות

חומר : פליז	תאריך	שם	תיכון ושירותים INSTRUMENT DESIGN שרותי מחקר WEIZMANN INSTITUTE OF SCIENCE		חלק תכנית	
כמות : 1	עודכן 28-05-97					
	שרטט 05-97 יהושע		מזמין : פיסיקה של חלקיקים		3561:00	SOREQ FEL סורק שדה מגנטי

Wiggler תיאור כללי של

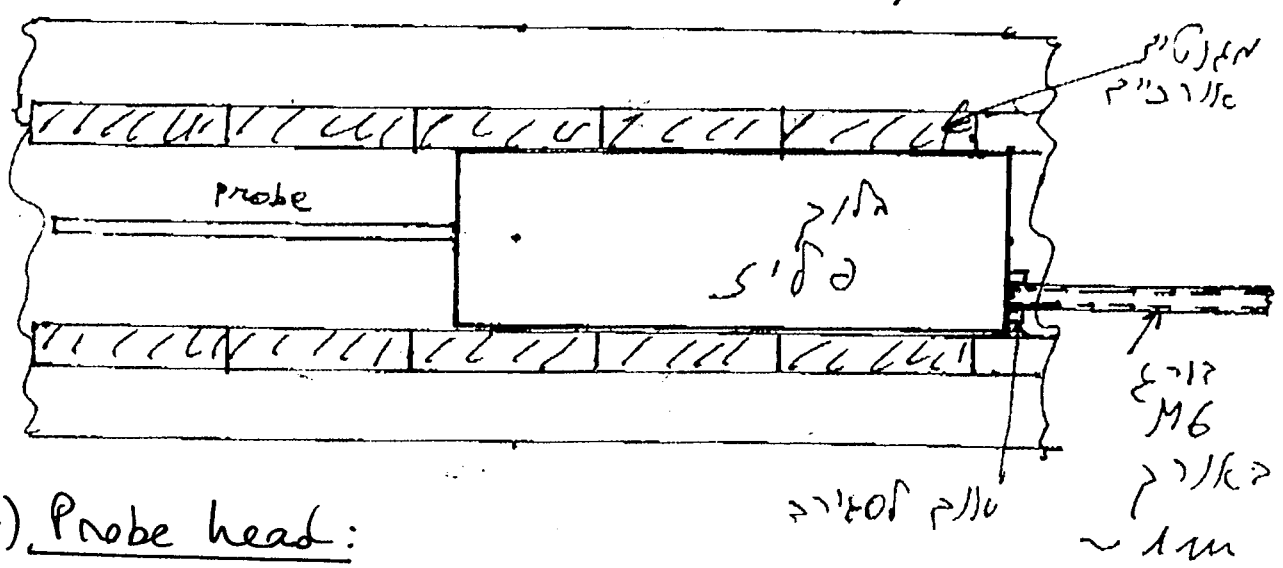

(a) Probe head:

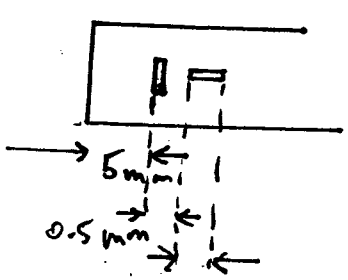

Fig. 2

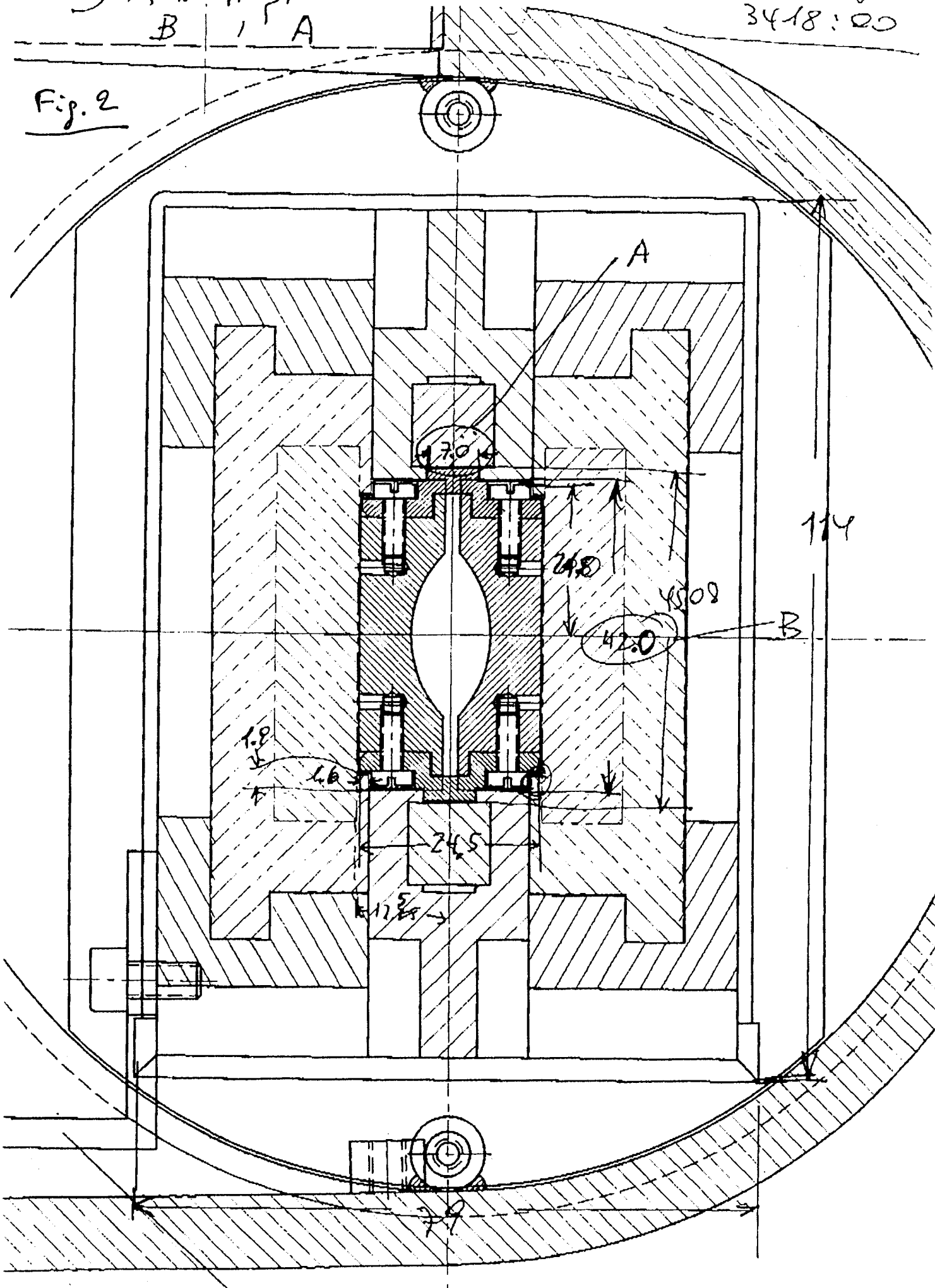

measurements near the end of the wiggler, rotate the wiggler by 180^0 around the vertical (x) axis, and pull again the block, measuring the field of the wiggler "backward" from out of its end back to the point where the first measurement was interrupted.

Figure 3:

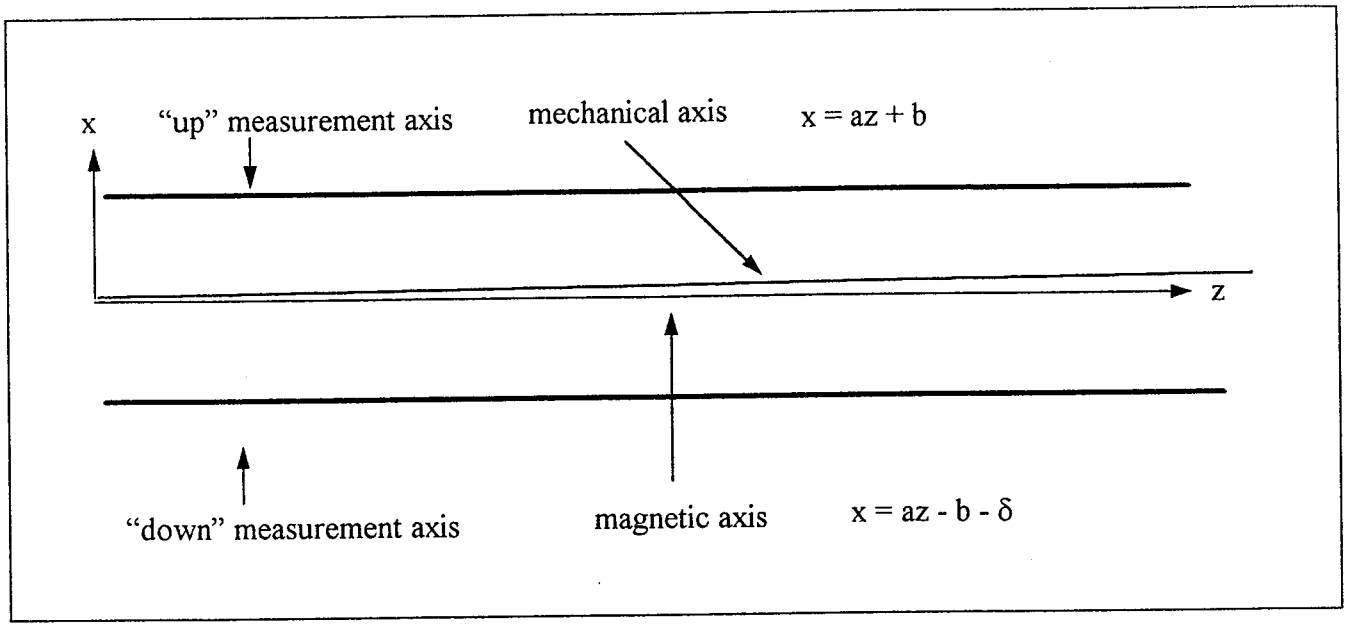

2. Measurement results

The transverse (By) and axial (Bz) magnetic fields measured in the "up" and "down" positions, are shown in Figs. 4,5.

The data was taken with steps of 1screw turns (one turn was supposed to correspond to 1 mm, later this was found to be inaccurate).

In all 4 measurements the first data point was taken when the probe end stuck out 100 mm off the face of the edge magnet of the wiggler. In the front measurement steps (Fig. 4a,5a), the first data point was marked - 100 mm, and the last data point was marked +942 mm. In the back measurement steps the first data point (largest coordinate) was marked arbitrarily 1300 mm and the last data point (smallest coordinate) was marked 929 mm (Fig. 4b) and 936 mm (Fig. 5b). Assuming that the wiggler length is 1201.5 mm (magnets face to face) and that the transverse field Hall probe chip position is 5.75 mm from the probe tip we can determine that

a. The first data point in the "front" measurements (marked - 100) corresponds to a point:
   - 94.25 mm relative to the first magnet face, or
   - 695 mm relative to the wiggler center

b. The last data point of the "back" measurements (marked - 1300) corresponds to a point:
   + 94.25 mm relative to the last magnet face, or

"up"

forward measurement Chart 2

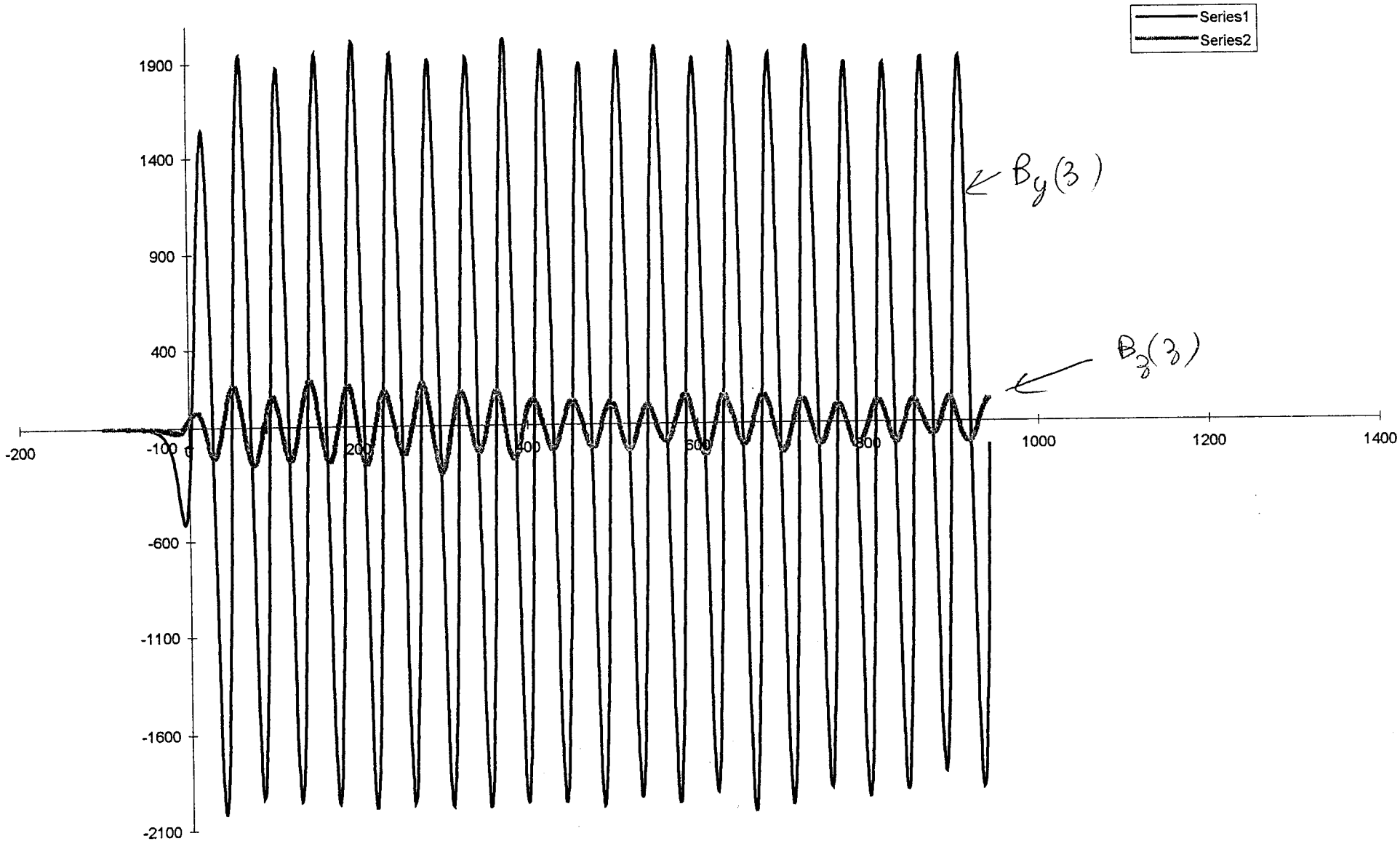

Fig. 4a

backward measurement Chart 2

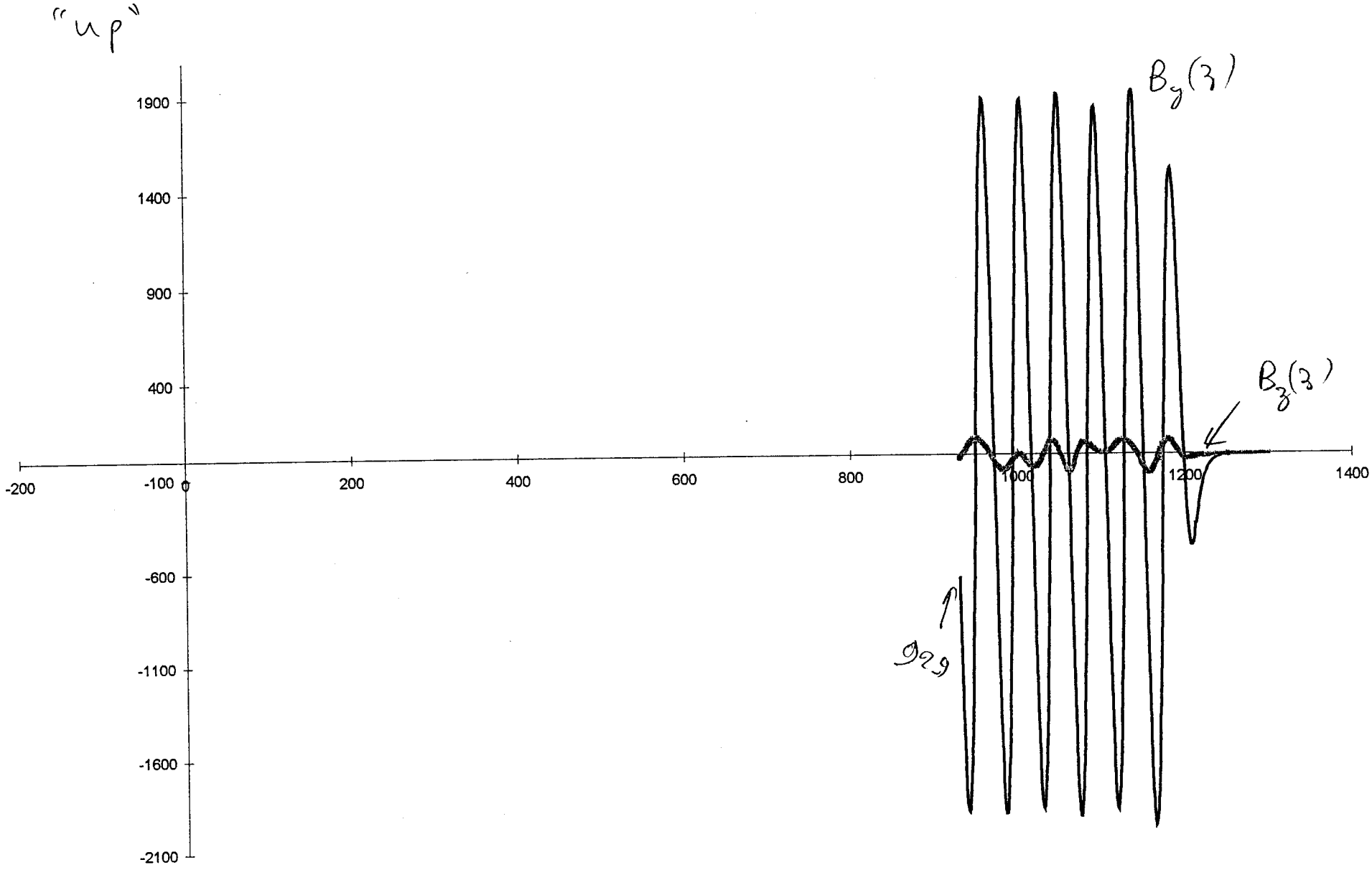

Fig. 4b

forward measurement Chart 1

down

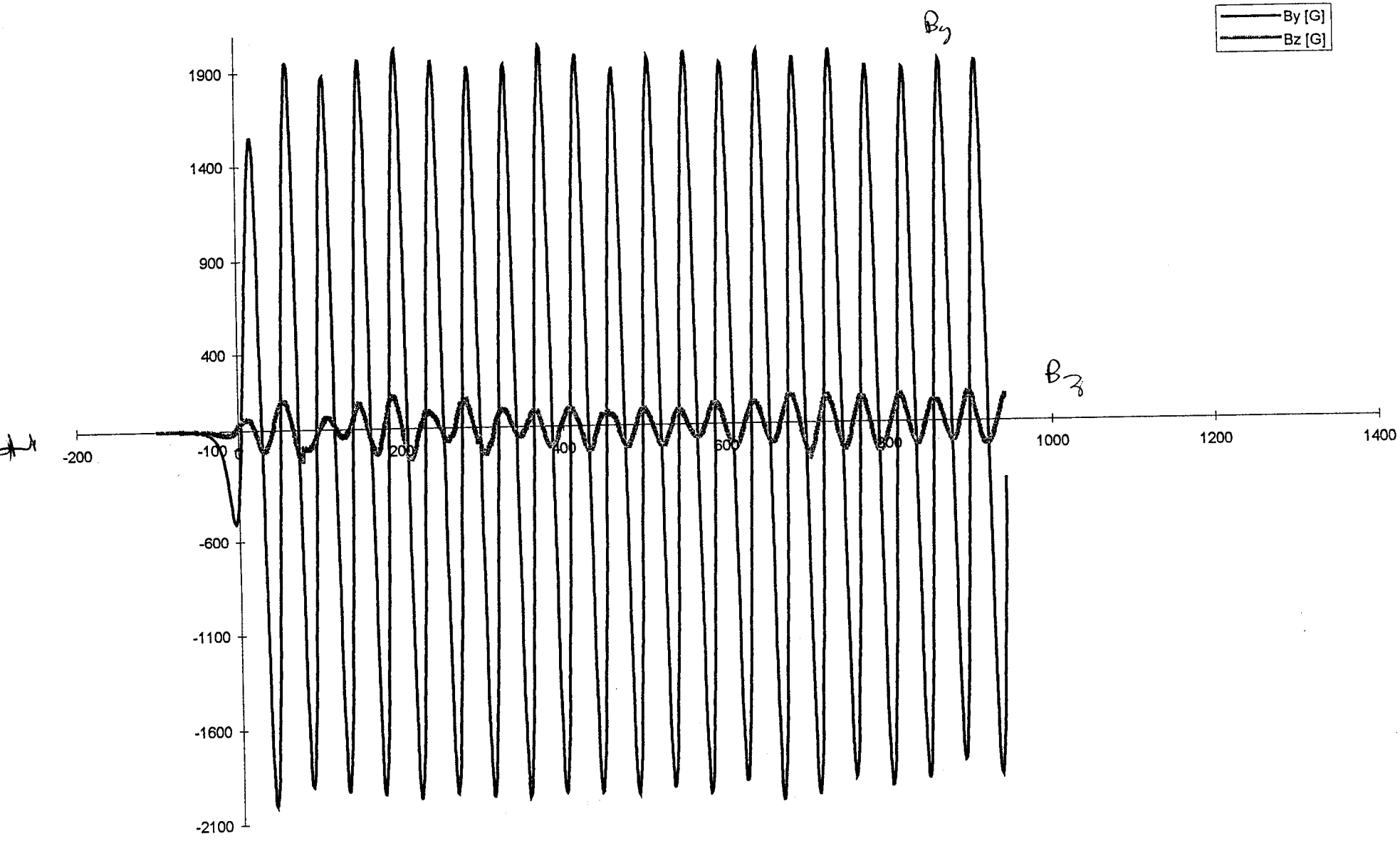

Fig 5 a

screws down

backward measurement Chart 1

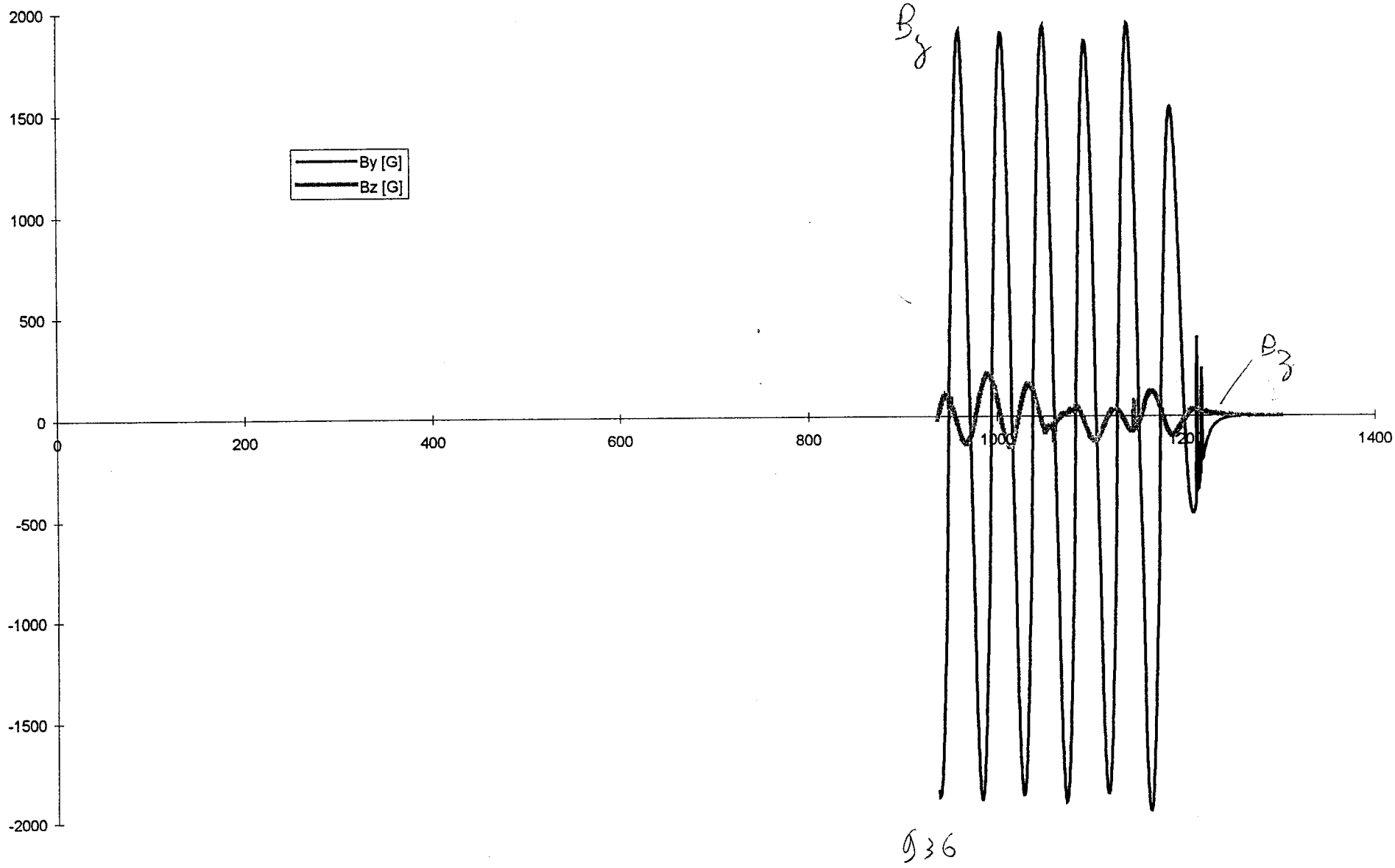

Fig. 5b

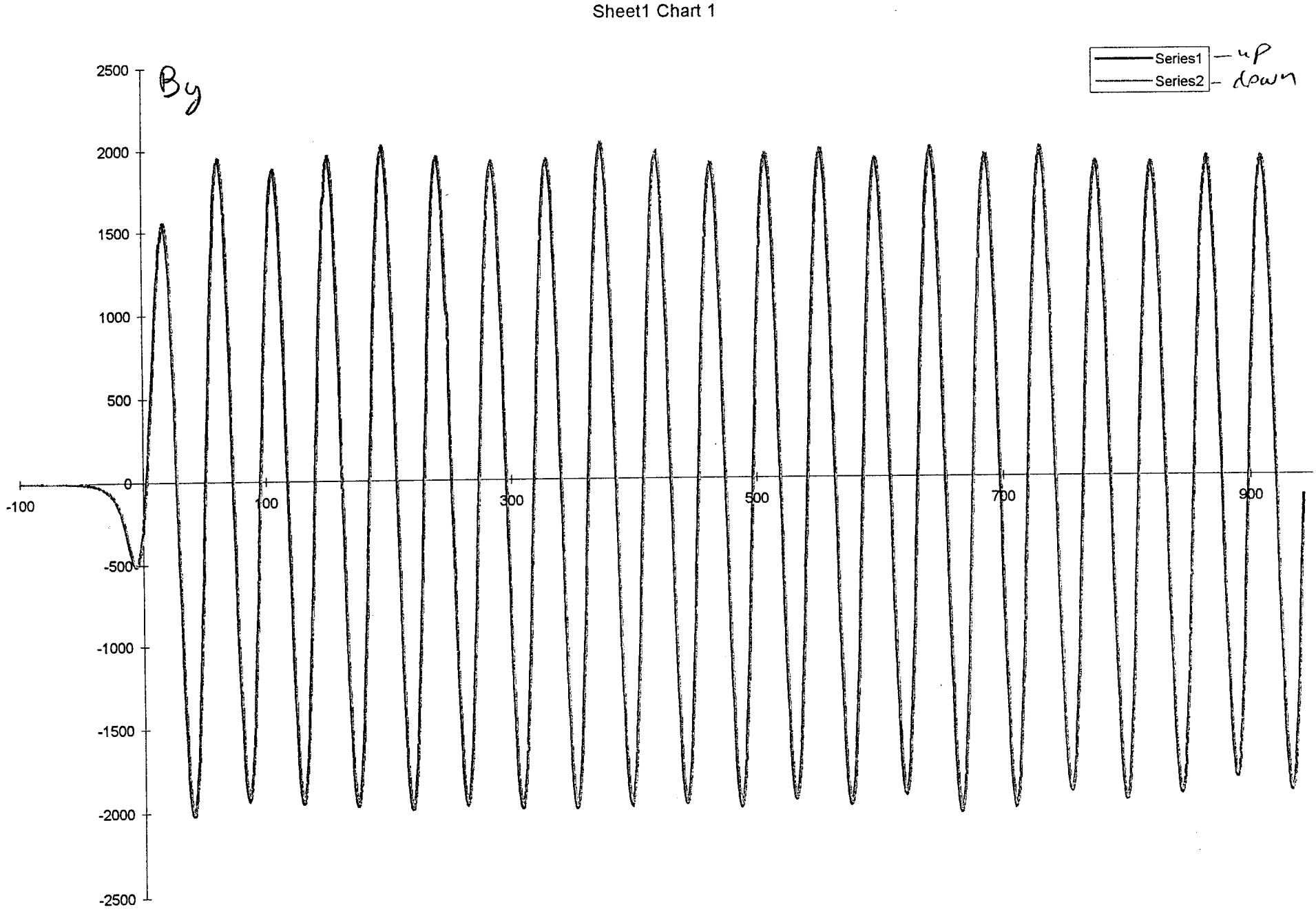
Sheet1 Chart 1
Series1
Series2
up
down
By
2500
2000
1500
1000
500
0
-500
-1000
-1500
-2000
-2500
-100
100
300
500
700
900

Fig. 6a

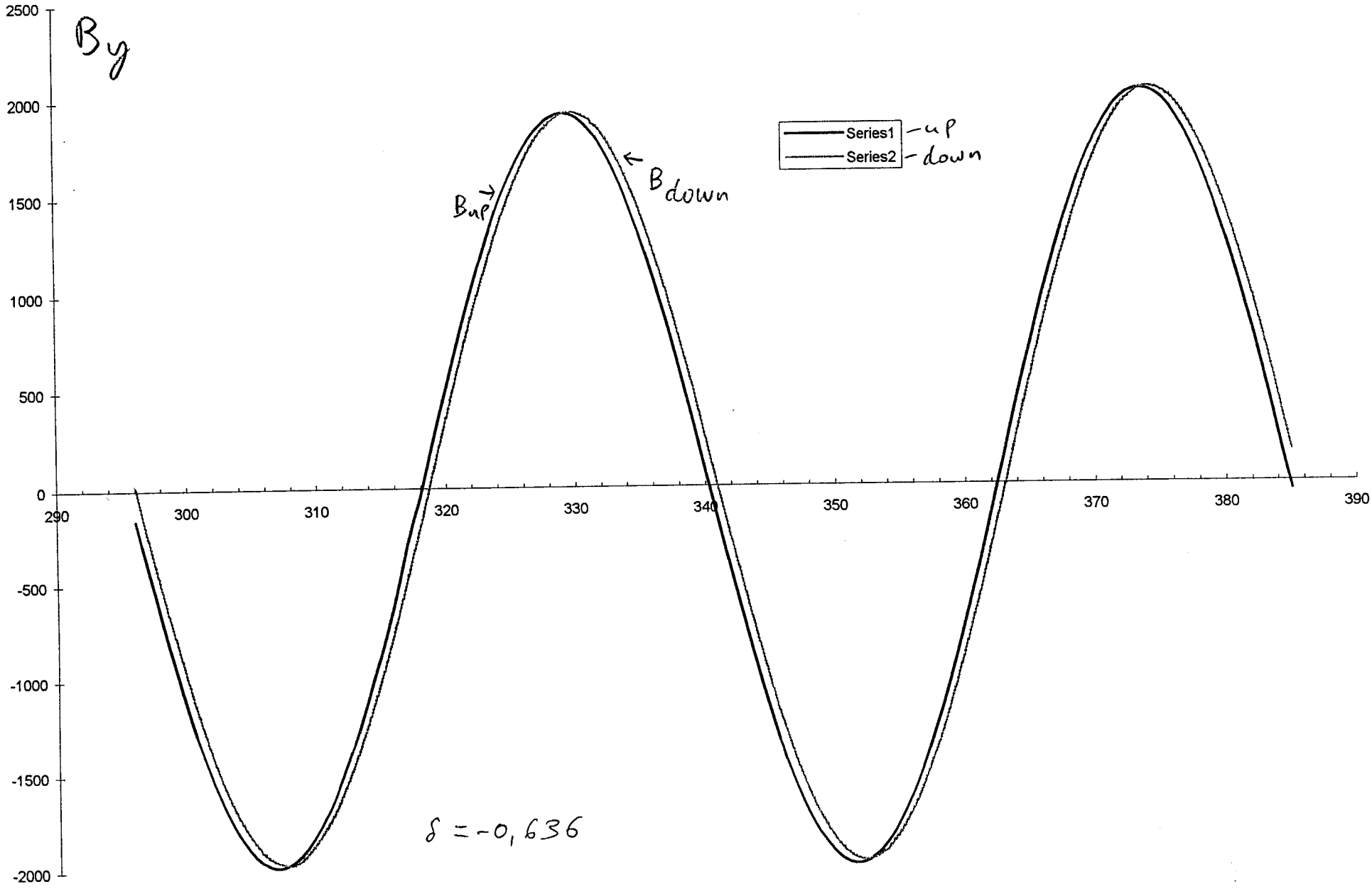
B_y
2500
2000
1500
1000
500
0
-500
-1000
-1500
-2000
290
300
310
320
330
340
350
360
370
380
390
Series1 – up
Series2 – down
B_{up}
B_{down}
$\delta = -0,636$

Fig. 6

+ 695 mm relative to the wiggler center

Later we found that the screw pitch was not exactly mm and the measurements steps and their origin were found by fitting the data to the known sinusoidal field $B_0 \cdot cos\left(\frac{2\pi}{44.44} z\right)$ relative to the wiggler center. We expect that after the readjustment at least the first data points will fit the above values within 0.5 mm accuracy.

Drawing of Bu(z) and Bd(z) on the same coordinate system (Fig. 6a) reveals the high accuracy of the measurement and its repeatativity. It also shows that magnet imperfection effects (small deviations of the wiggling amplitudes along the axis) are slowly varying and are the same on the upper and lower axis.

Closer examination of a magnified section (Fig. 6b) reveals a small error in determining the origin of measurements Bu(z) and Bd(z). The origin of Bd(z) is 0.636 mm ahead of Bu(z) (determined by correlation).
Note that the curve Bd(z) is slightly higher than Bu(z) indicating that

$$\alpha = \frac{\partial B_y}{\partial X} = \frac{B_y^{up} - B_y^{down}}{\delta} < 0$$

This result is consistent with the observation that the magnetic field of the upper (+x) longitudinal magnets is in the +y direction and the magnetic field of the lower (-x) ones is in the -y direction. The fringe fields of such a magnet configuration indeed generates a negative gradient $\partial By/\partial x$.

The axial magnetic field (Bz) measurements of the up and down (front) measurement steps are displayed in Figs. 7a,b,c on the same coordinate system. The two curves are much less regular in comparison to the By measurements and their difference is not insignificant (especially near $z \approx 100$ mm).

A puzzling effect is the large shift of the "up" curve relative to the "down" curve (approximately 2 mm). We would expect to get the same shift as for the By(z) measurements (≈ 0.6 mm). This excessive shift is yet unexplained.

7. Measurement accuracies

The bronze block was fitted into the wiggler frame with 0.1 mm freedom in the transverse dimensions to enable smooth sliding. Relying on the heaviness of the block and assuming the frame is smooth, the accuracy in the transverse position is $\Delta x = \Delta y = 0.1$ mm. Considering that the probe protrudes out of the block 110 mm, while the block length is 150 mm, one can also imagine extreme cases when the block tilts $\pm$ 0.1/150 rad, and thus the probe deviates $\Delta x = \Delta y = \pm 0.2$ mm

If the probe is not straight, or if the probe is not parallel to the frame, this can cause a systematic error in the probe movement axis position which will be offset to the other side (in both x and y dimension) when the block is rotated. However knowing the

Sheet1 Chart 1

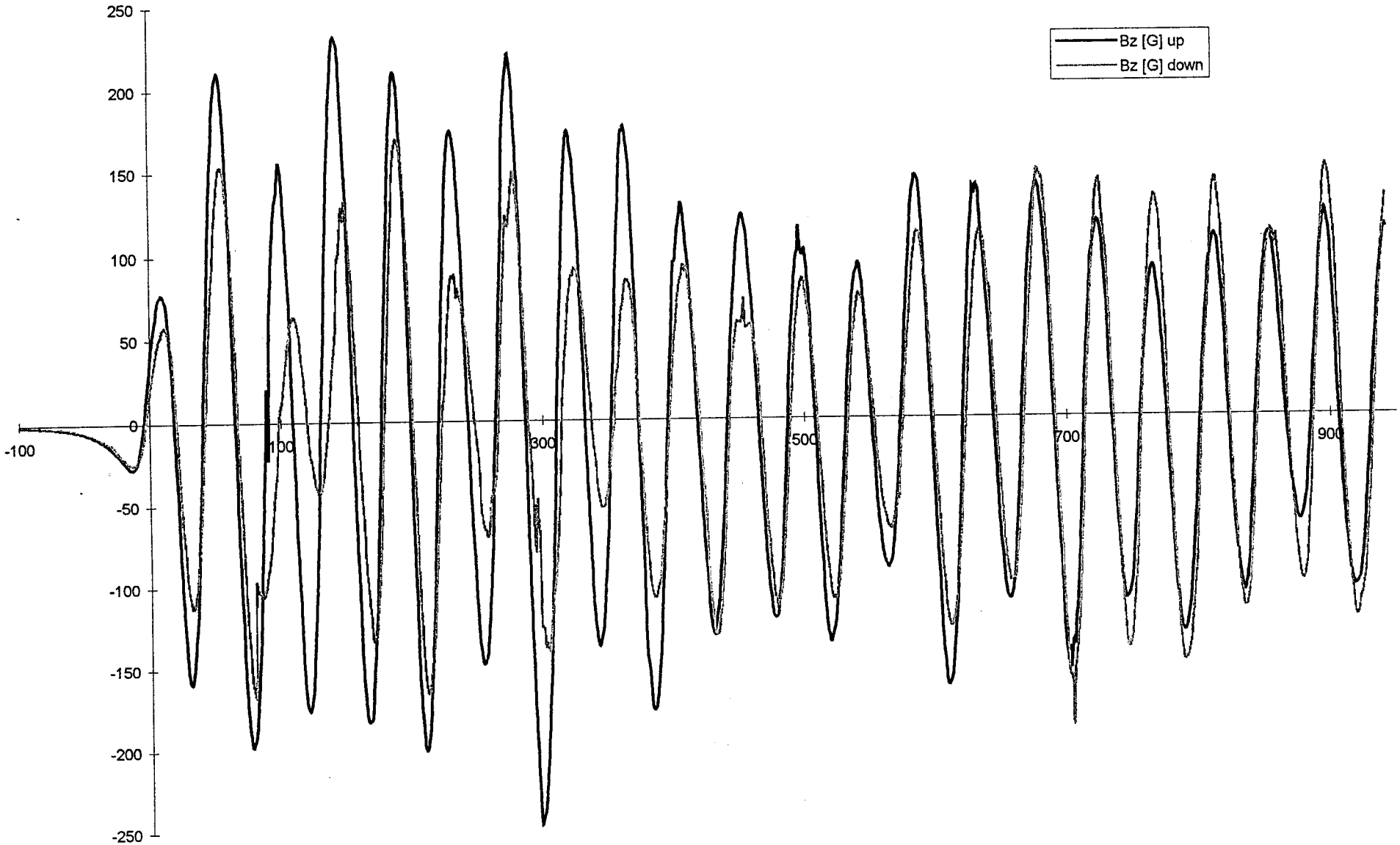

Fig. 7a

Sheet1 Chart 1

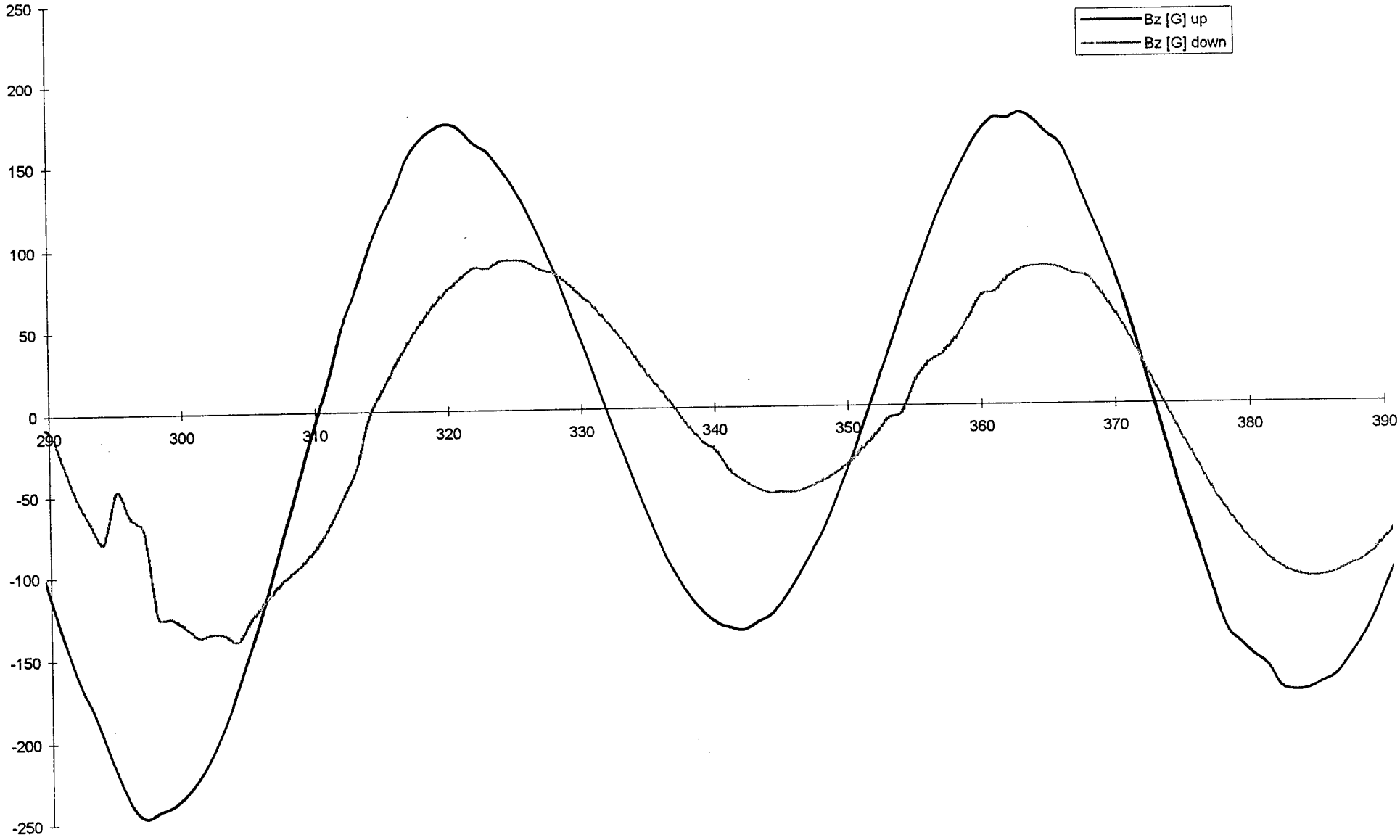

Fig 7

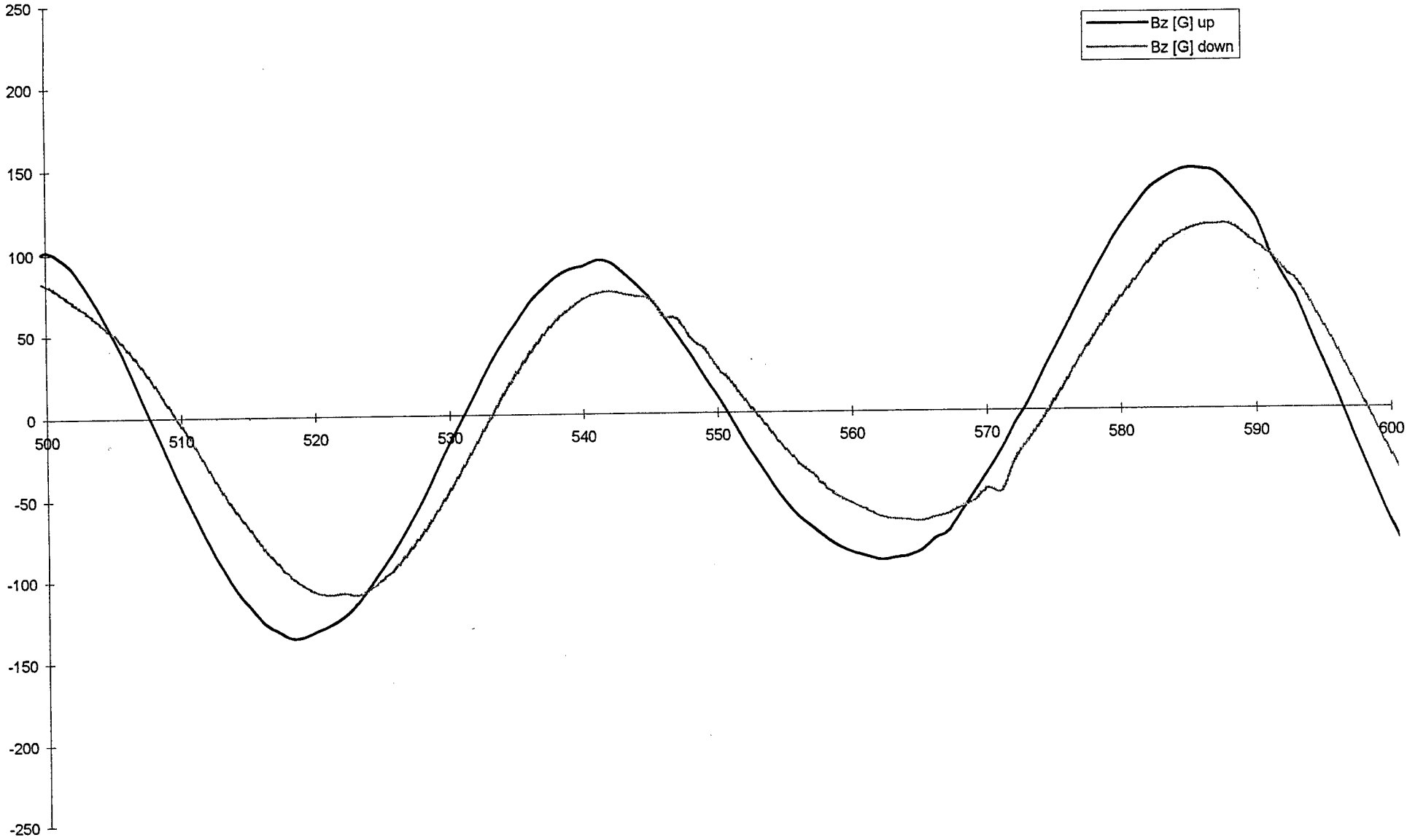
Bz [G] up
Bz [G] down
250
200
150
100
50
0
-50
-100
-150
-200
-250
500
510
520
530
540
550
560
570
580
590
600

Fig. 7C

transverse displacement of the probe only with accuracy 0.4 ± 0.2 mm may lead to a poor estimate of the gradient α.

The axial displacement measurement of the long screw was determined by measuring a 1m length section of the screw accurately with a caliper, and then counting turns (Kanter and Gover - July 14, 1997). We found:

1004 turns = 1000 mm
namely: 0.9960 mm/turn

As we will see later, best fit between the data and sinusoidal function gave a period 44.60 turns. Since we confirmed that the periodically of the wiggler is $\lambda_w = 44.44$ by total length measurement (report of 15.6.97), we get:

44.60 turns = 44.44 mm
namely: 0.9964 mm/turn

This is quite close to the previous measurement (the difference corresponds to 0.7 mm over 1200 mm).

Earlier measurement by Sokolowski (on a lace) gave:
550 turns = 549.6 mm
namely: 0.9993 mm/turn

A possible explanation for the discrepancy is that the screw that is composed from two welded sections was made from two different screws. This results in a systematic measurement accuracy. We will still use the factor 0.9964 as the correction factor that gives best average fit.

8. Determination of the y deviation of the magnetic axis

An appropriate model for the wiggler magnetic field away from the ends is

$B_x = 0$
$B_y = B_0 \cosh(k_w y) \cos k_w(Z-Z_0)$
$B_z = -B_o \sinh(k_w y) \sin k_w(Z-Z_0)$
It satisfies $\underline{\nabla} \cdot \underline{B} = 0$, $\underline{\nabla} \times \underline{B} = 0$.
For $k_w Y_0 << \pi$
$B_y = B_0 \cos k_w(Z-Z_0)$
$B_z = -B_0 k_w Y_0 \sin k_w (Z-Z_0)$

Clearly $B_z(z) = 0$ on axis and has a 90^0 phase shift relative to $B_y(z)$ off axis:

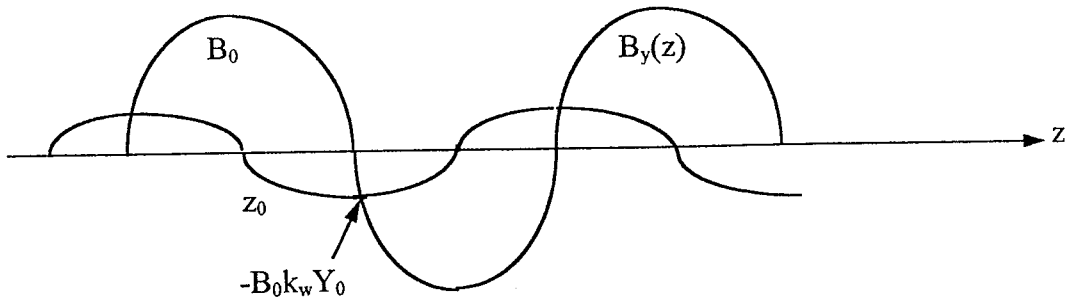

Fig. 8

Phase shift of B_z relative to B_y:
-90^0 for $Y_0 > 0$
$+90^0$ for $Y_0 < 0$

In Figs. 4a,5a,b, clearly the situation is the first case, hence we may assume that the probe sliding axis is shifted relative to the magnetic axis in the y direction. The shift can be estimated from

$$\frac{B_y(y_0, z_0 - \lambda_w/4)}{B_y(y_0, z_0)} = \frac{B_0 k_w Y_0}{B_0} = 2\pi \frac{y_0}{\lambda_w}.$$

$$2\pi \frac{Y_0}{44.44} \cong \frac{150\text{Gs}}{2000\text{Gs}} = 0.075$$

$Y_0 \cong 0.53$ mm

Fig. 4b ("up-back" measurement) is exceptional to the other curves, since in this case $B_z(z)$ is $+ 90^0$ out of phase with $B_y(z)$ which suggests $Y_0 < 0$. This is either a result of wrong polarity recording, or a big shift in the y position of the probe due to the freedom of the block in its frame.

It is somewhat surprising that the phase shift is the same in the "up" "front" and "back" measurements (Fig. 4) and the "down" "front" and "back" measurements (Fig. 5) both the radiation of the wiggler and the rotation of the block should change the shift from $+Y_0$ to $-Y_0$ if the probe is off - center. This indicates that the probe is positioned well in the center of the frame and does not change its position when the block or wiggler is rotated. A possible explanation is that the wiggler magnets on the +y side are further from the mechanical axis than the -y magnets or weaker. Another explanation is an error in recording the field sign.

9. Gluing the front and back data

Our goal now is to glue the front and the back measurements data and determine accurately the absolute positions of the origin of all four measurements.

The first step was to determine the periodicity of the measured field in the "up-front" measurement step by applying EXCEL solver on the minimization problem:

$$\min_{\lambda_w} \sum_{i=1}^{N} \left[B_y^{up}(z_i) - B_0 \cos\frac{2\pi}{\lambda_w}(z - z_0) \right]^2$$

where B_0 = 1945 Gs and z_1 = 100, z_N = 942 are two points far from the ends of the wiggler.

This procedure resulted in
λ_w = 44.6015 mm
a result which is quite surprising since our current estimate of the wiggler period
λ_w = 44.44 mm, fitted very well (within less than 0.5 mm) the recent measurements of the entire wiggler length (1201.5 mm). An error of 0.14 mm per period corresponds to a 4 mm error in the wiggler length, which is not expected. We relate this error to inaccuracy of the screw pitch (see section7) and decided to readjust the axial position data of all measurements by multiplying their axial position coordinate (given in terms of screw turns) by a factor

$$\frac{44.44}{44.6015} = 0.9964 \text{ mm/turn}$$

After this rescaling step we shifted the origin of all four measurements so that the data will be given relative to a common origin, which we determined to be in the center of the wiggler (600.75 mm from both ends). This was done by finding

$$\min_{z_0} \sum_{i=1}^{N} \left[B_y^{meas}(z_i - z_0) - B_0 \cos\frac{2\pi}{\lambda_w}(z - 0) \right]^2$$

for B_0 = 1945Gs, λ_w = 44.44 mm . We found

up front	z_0 = 594.50	z_{-100} = -694.13
down front	z_0 = 595.1367	z_{-100} = -694.77
up back	z_0 = 601.0861	z_{-1300} = 694.2
down back	z_0 = 600.70	z_{-1300} = 694.6

The last column corresponds to the first data points that were taken in all four measurements when the probe end protruded 100 mm off the wiggler and the probe sensor was at coordinate ± 695 mm relative to the wiggler center (see sect. 2). The discrepancy -(0.3-0.9) mm is within the measurement accuracy and indicates that the "rescaling" and "origin shift" are reasonable.

The matching of the data to the $B_0\cos(2\pi/\lambda_w \cdot z)$ function was verified by inspecting both curves on the same coordinate system. Figs. 9a,b show the matching quality to the cosine function for the "up-front" and "up-back" data respectively.

The readjusted "front" and "back" EXCEL data files of the "up" measurement (written in terms of axial position coordinates relative to the wiggler center with spacing of 0.9964 mm) were merged and the data points where put in sequence (using "SORT") so

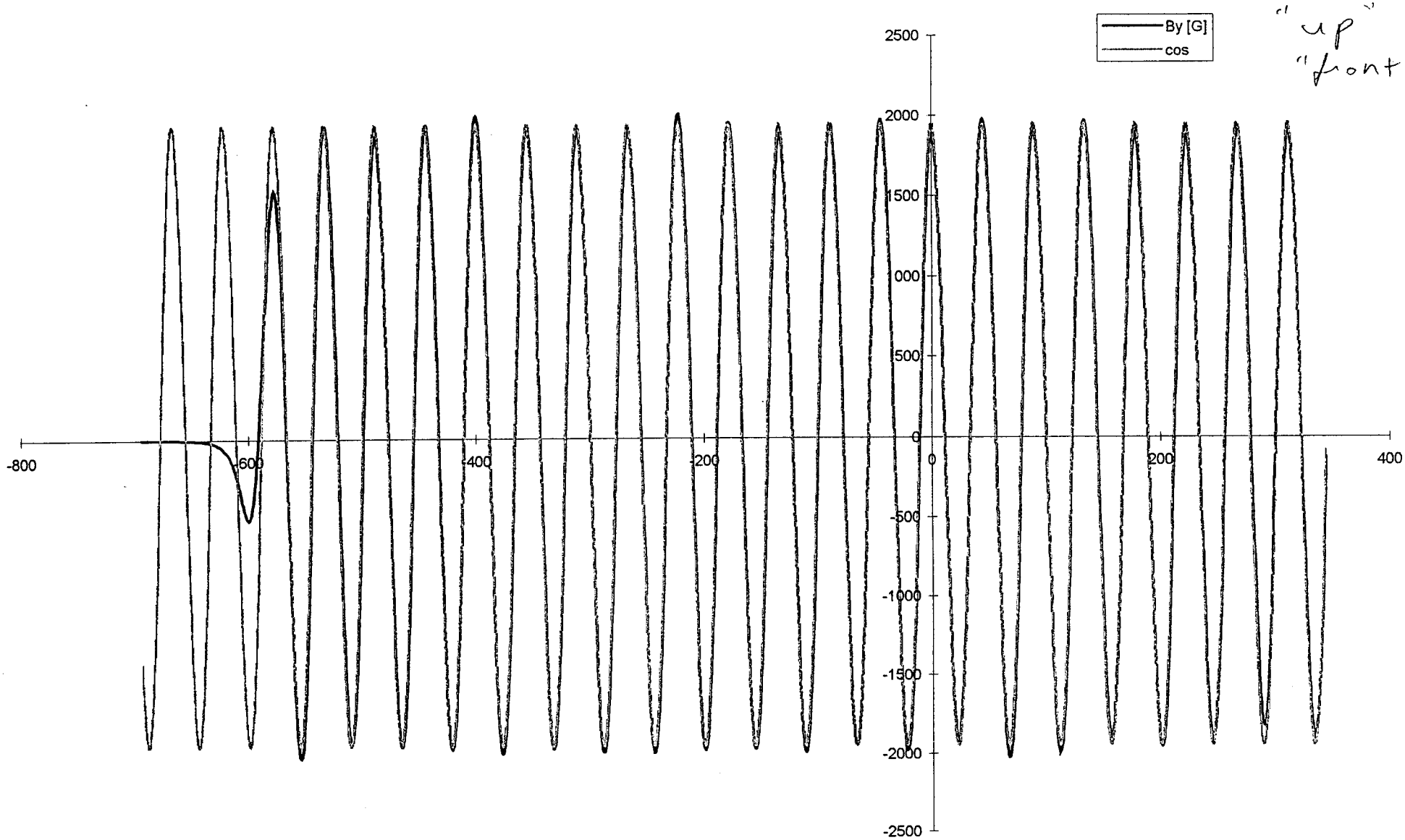
By [G]
cos
2500
2000
1500
1000
500
0
-500
-1000
-1500
-2000
-2500
-800
-600
-400
-200
0
200
400
"up"
"front"

Fig. 9a

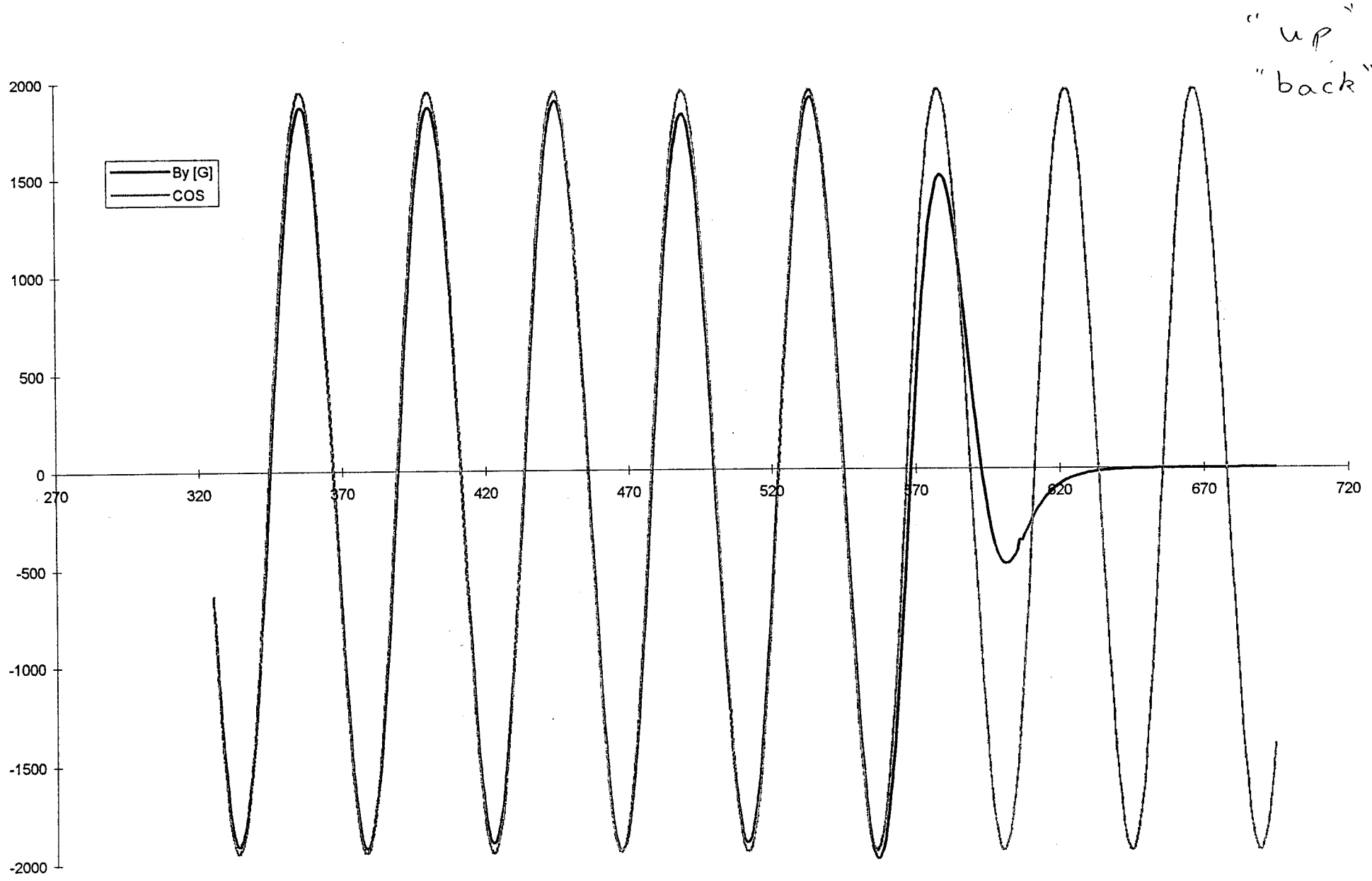
"up"
"back"
By [G]
COS
2000
1500
1000
500
0
-500
-1000
-1500
-2000
270
320
370
420
470
520
570
620
670
720

Fig. 9b

that the front and back data points interlaced in the small overlap section. Fig. 10 shows the merged data which seems seamless!

To examine the quality of the match we added in EXCEL the "back-up" measurement data array to the end of the "front-up" array and drew the overlap region (yet before the "SORT" step). Fig. 11 shows the quality of the match. The two curves shift by less than 0.1 mm from each other.

The mismatch of the bottom data is much bigger as seen from Fig. 12a (0.2-0.3 mm). To determine which set deviates more from the cosine behavior we also draw the $B_0 \cdot \cos\left(\frac{2\pi}{44.44} z\right)$ curve on the same coordinates (Fig. 12b). This does not help, because the cosine amplitude seems to be too large (or the data is shifted by a constant field). To make the comparison possible we readjusted the cosine amplitude to B_0 = 1900Gs( ) (Fig. 12c). The cosine shows now a good match to the "backward" curve. The shift is of the "forward" curve. This should be, perhaps rechecked again in different regions after finding the field on axis.

10. Determination of the field gradient

The magnetic field along the up and down measurement axes can be described as a sum of three contributions:

a. the magnetic field generated by ideal wiggler magnets: $B^{id}(z)$,

b. the fields generated by magnet defects: $B^{def}(z)$

c. the field generated by the longitudinal magnets: $B_y^{grad} = \alpha x$.

$$B_y(z) = B_y^{id}(z) + B_y^{def}(z) + B_y^{grad}(z)$$

substituting

$x = az + b$	for the "up" measurement axis
$x = az + b - \delta$	for the "down" measurement axis

we have:

$$B_u(z) = B_u^{id}(z) + B_u^{def}(z) + \alpha(az + b)$$
$$B_d(z) = B_d^{id}(z) + B_d^{def}(z) + \alpha(az + b - \delta)$$

Because the wiggler field and the defects field do not change much as a function of the transverse dimensions

$$B_u^{id}(z) \cong B_d^{id}(z) = B_{axis}^{id}(z)$$
$$B_u^{per}(z) \cong B_d^{per}(z) = B_{axis}^{per}(z)$$

Within a section $z_1 < z < z_2$ inside the wiggler, where z_1, z_2 are at least one period away from the wiggler ends the field $B^{id}(z)$ is periodic

$$B^{id}(z) = B_0 \cos k_w(z - z_0) + \{\text{harmonics}\}$$

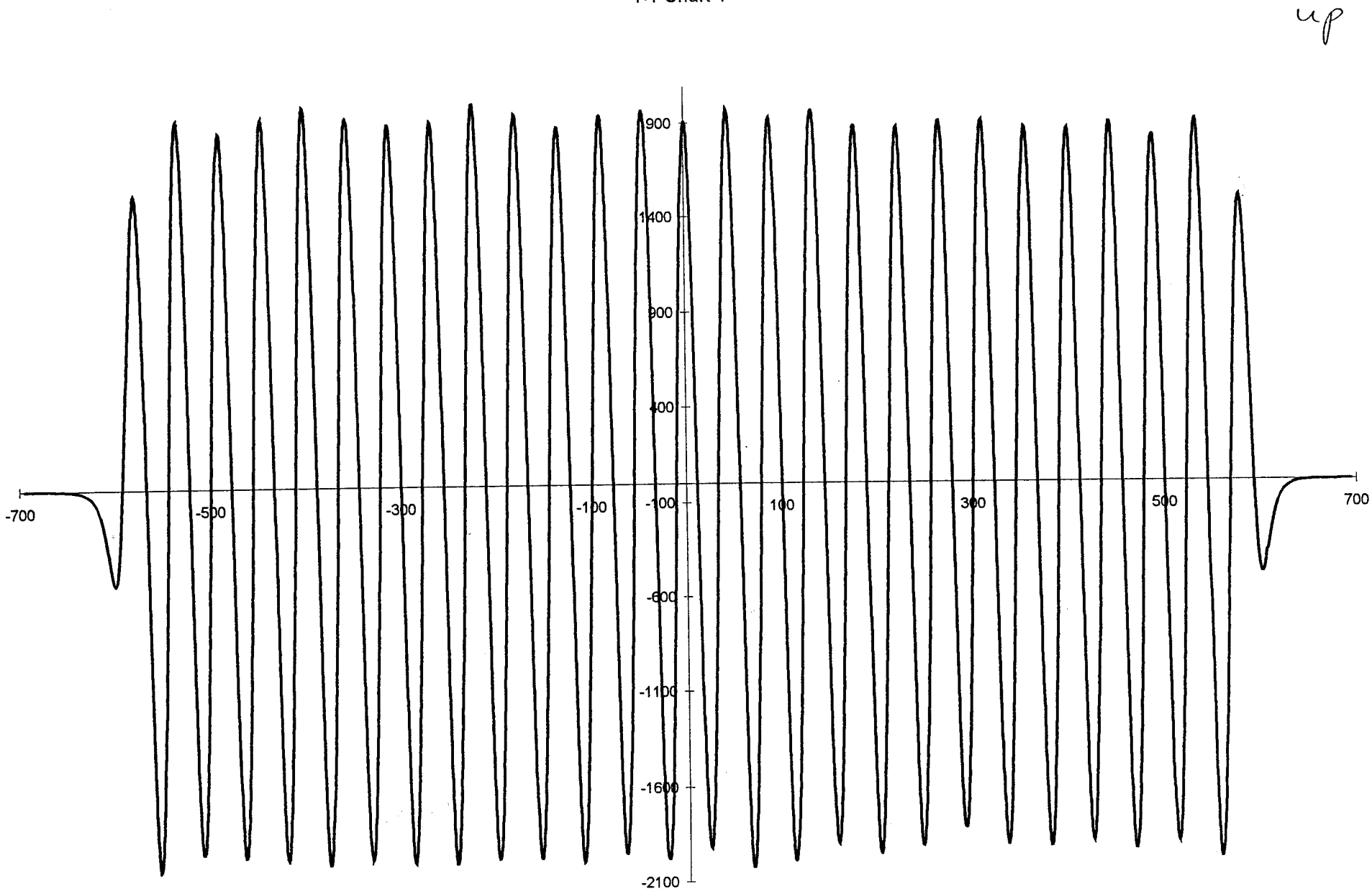
I+r Chart 1
900
1400
900
400
-100
-600
-1100
-1600
-2100
-700
-500
-300
-100
100
300
500
700

up

21

Fig. 10

up

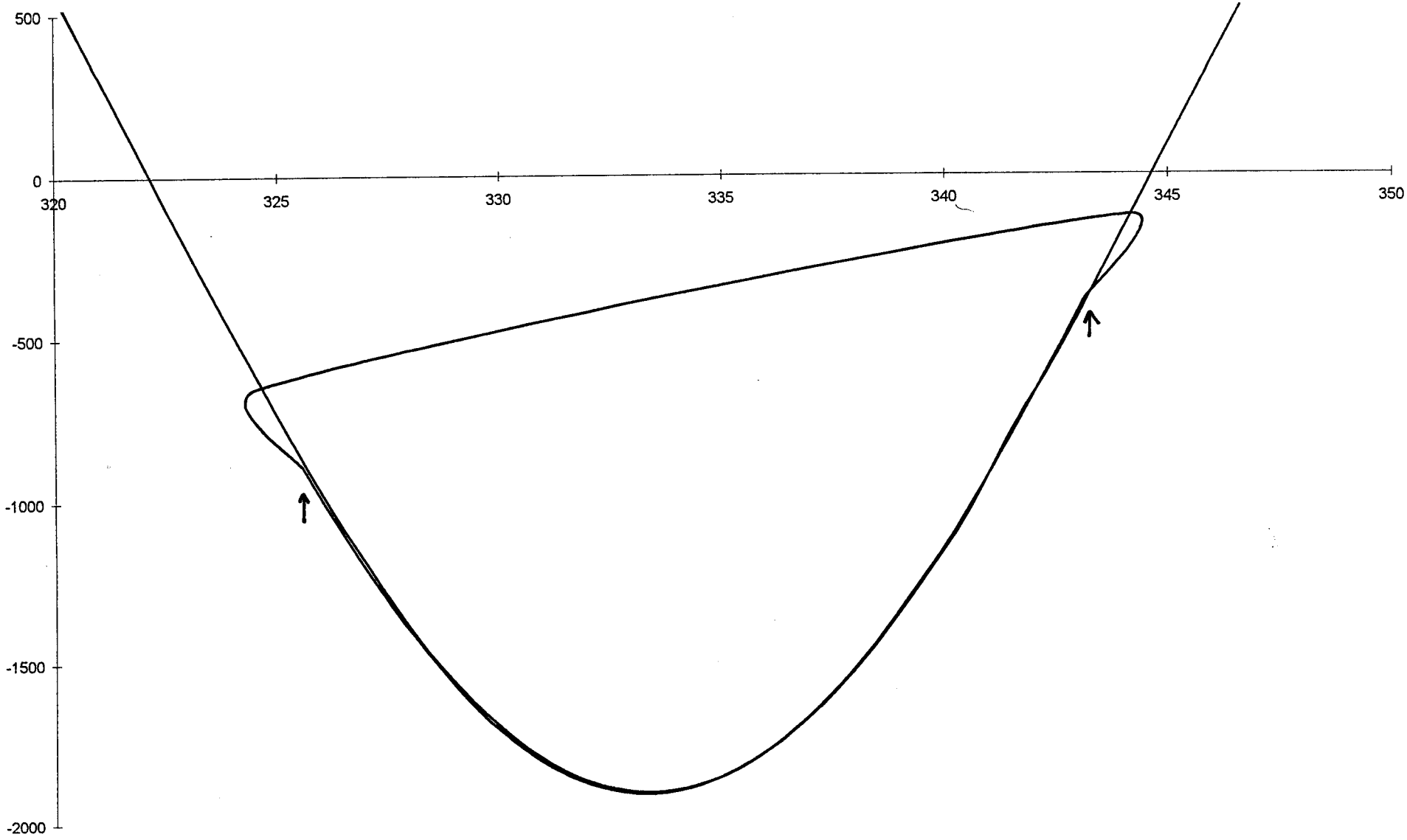

99

Fig. 11

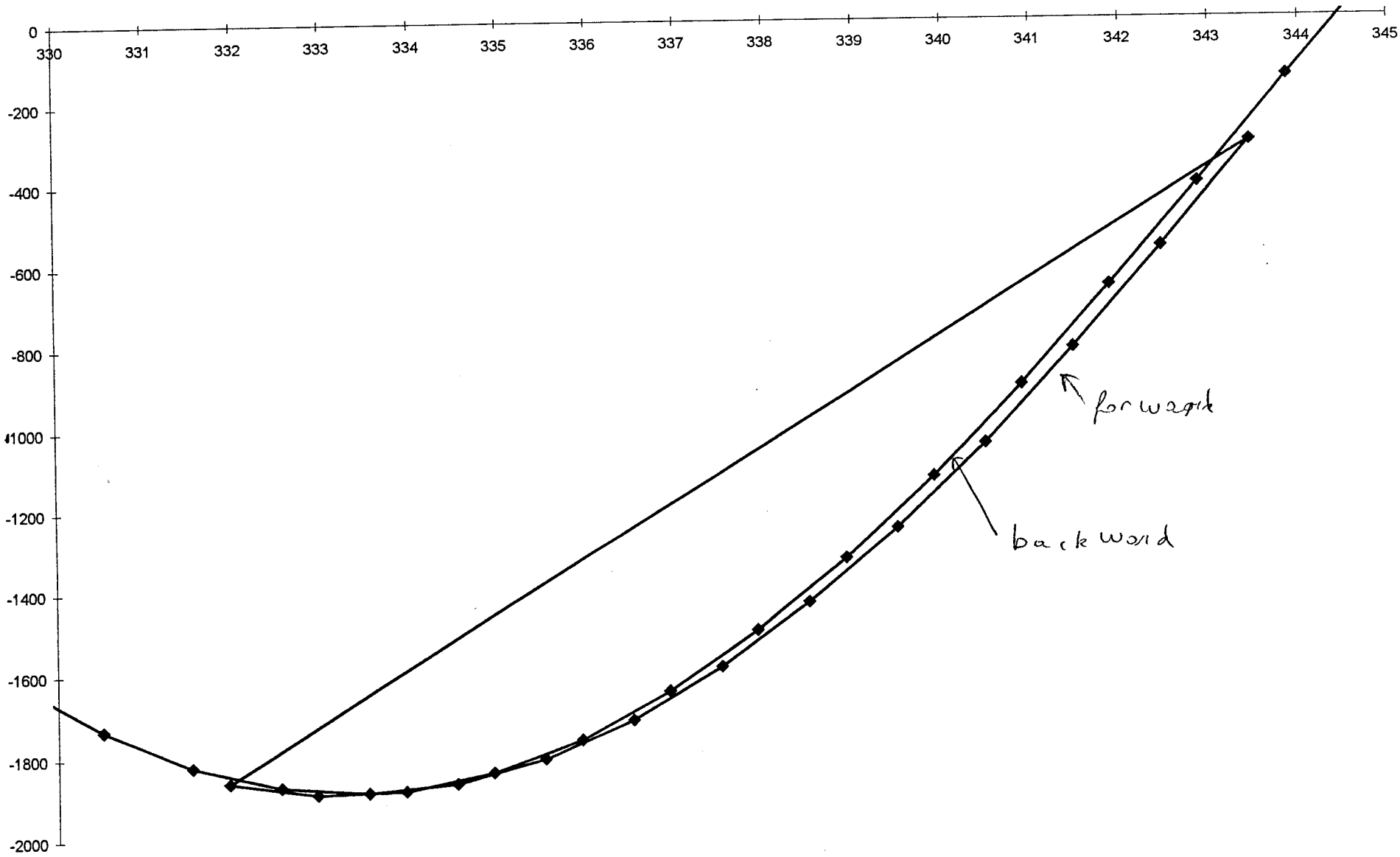
Sheet1 Chart 1
down
0
-200
-400
-600
-800
-1000
-1200
-1400
-1600
-1800
-2000
330
331
332
333
334
335
336
337
338
339
340
341
342
343
344
345
forward
backward

Fig. 12a

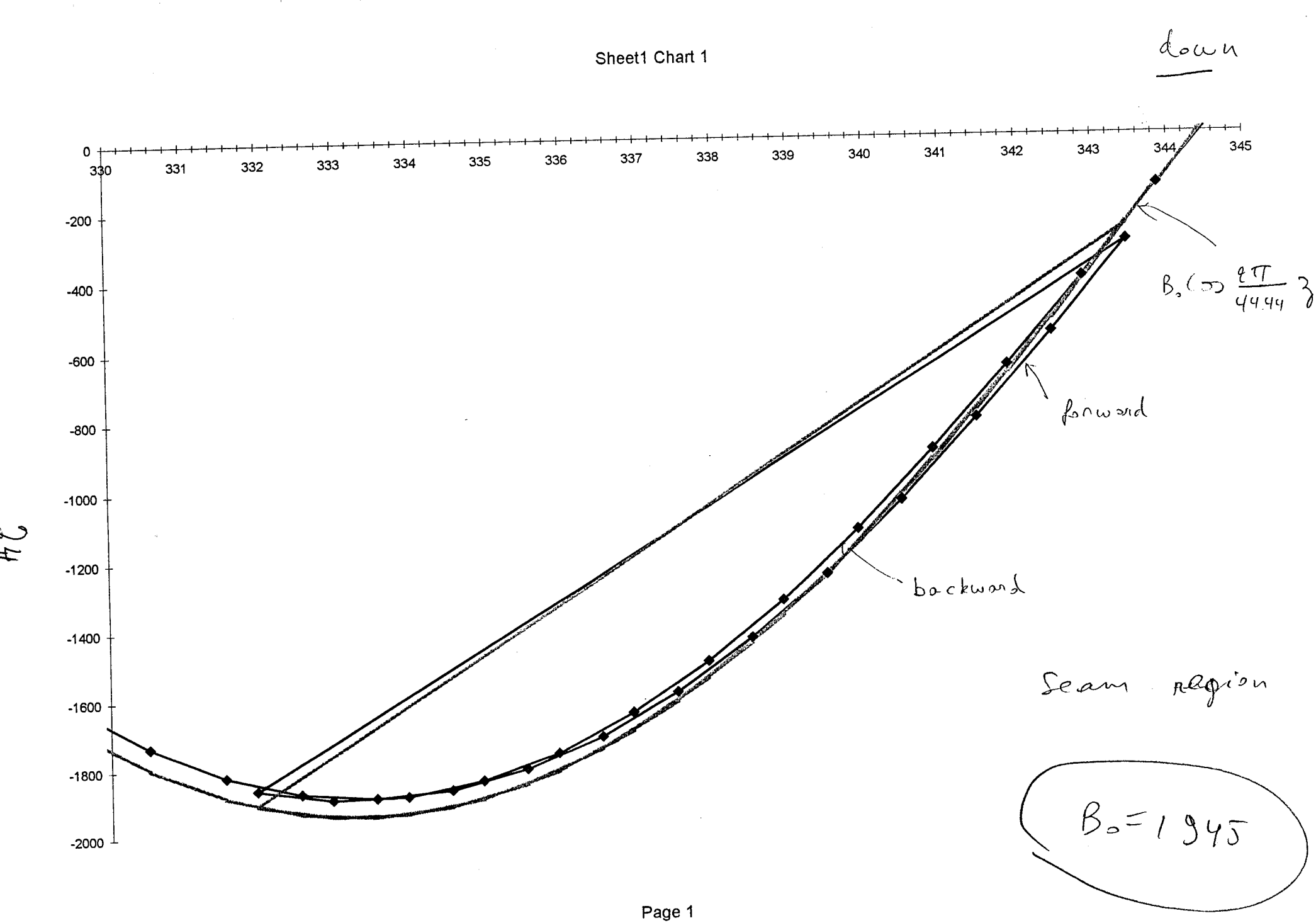
Sheet1 Chart 1
down
0
330
331
332
333
334
335
336
337
338
339
340
341
342
343
344
345
-200
-400
-600
-800
-1000
-1200
-1400
-1600
-1800
-2000
$B_o = \frac{qT}{4444}$ 3
forward
backward
Seam region
$B_o = 1945$
Page 1

Fig. 12 b

down

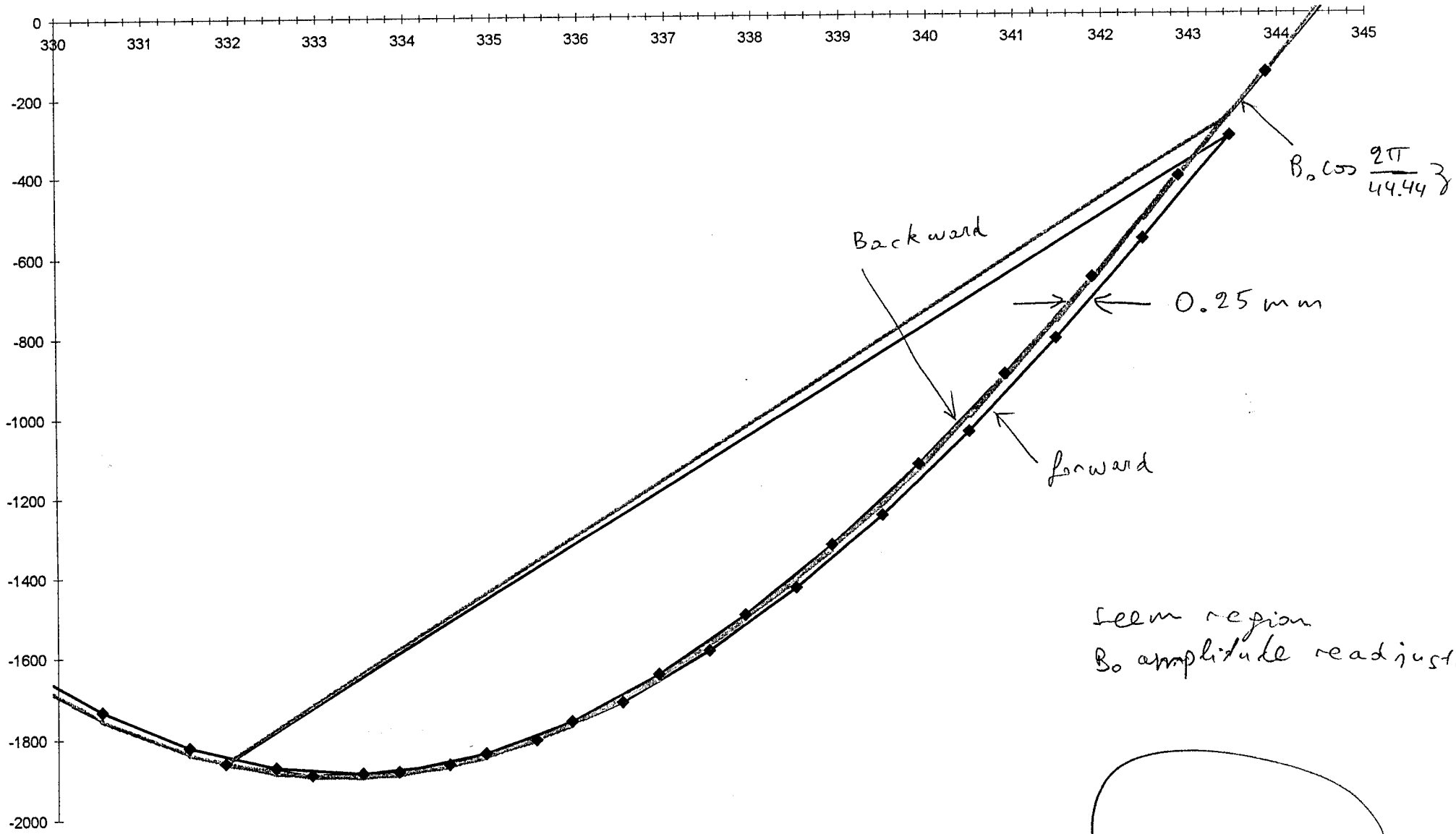

Seem region
B_0 amplitude readjusted:

$B_0 = 1900$

Fig. 12c

In order to compute the three field components we take advantage of the "harmonics filtering" transformation:

$$f^{av}(z) = \tau\{f(z)\} \equiv \frac{1}{\lambda_w}\int_{z-\lambda_w/2}^{z+\lambda_w/2} f(z')dz'$$

This transformation will erase $B^{id}(z)$ when applied between the limits $z_1 < z < z_2$. It leaves the linear function unchanged exactly:
$\tau\{az + z\} \equiv az + b$, and has little effect on the slowly varying field $B^{def}(z)$ (this assumption should be examined more carefully - the axial variation of single wiggler magnet defect fields can be of the order λ_w and the transformation may distort its, it is less likely to distort the slower varying fields due to the correction magnets).

With these assumptions we may estimate

$$B_u^{av}(z) = B_u^{def,av}(z) + \alpha(az+b) \cong B_u^{def}(z) + \alpha(az+b)$$
$$B_d^{av}(z) = B_d^{def,av}(z) + \alpha(az+b) \cong B_d^{def}(z) + \alpha(az+b-\delta)$$

In order to perform the suggested transformation numerically, we fed the merged data of the fields from Excel to Mathcad and performed a "Spline" transformation on it in order to turn the fields data into continuos functions. The spline transformation interpolates the data points using local third order polynomial fitting and interpolation.

The spline functions of the merged up and down data and the ideal field on axis calculated from El-op are drawn in Fig. 13. There is a reasonably good match of the curves all over.

Now we apply the filtering transformation on the entire data and display the result in Fig. 14. The spikes in the wiggler ends are of course insignificant and only the region -550 mm $< z <$ 550 mm contains significant information on the (somewhat distorted) defects field $B^{def}(z)$ and the gradient field $B_{up}^{grad}(z)$, $B_d^{grad}(z)$.
About 9 defect peaks are observed along the wiggler in both the average "up" and "down" curves (similar to the number of correction magnets along the wiggler). The "up" curve is almost consistently below the down curve indicating a negative gradient.

To determine the field gradient we subtract the fields: $B_u^{av}(z)$ - $B_d^{av}(z)$ and display the difference in Fig. 15. The mean field difference over the region $-600 < z < 600$ is:

$(\Delta B)_{av} = -13.2$ Gs
If we assume $\delta = 0.4$ mm, then $\alpha = -32.9$ Gs/mm

Closer examination of Fig. 15 reveals that there is a jump in ΔB around $z \cong 334$ mm which is the region of the "seam". If we average seperately in the front and back sections we obtain:
Front : $(\Delta B)_{av} = -10.9$ Gs $\alpha = -27.5$ Gs/mm (for $\delta = 0.4$ mm)
Back: $(\Delta B)_{av} = -20.9$ Gs $\alpha = -52.2$ Gs/mm (for $\delta = 0.4$ mm)

ORIGIN := 1

u := READPRN(t_up) d := READPRN(t_down) E := READPRN(t_elop)

i := 1 .. 1415 j := 1 .. 1396 k := 1 .. 1400

$zu_i := u_{i,1}$ $Bu_i := u_{i,2}$ $zd_j := d_{j,1}$ $Bd_j := d_{j,2}$ $ze_k := E_{k,1}$ $Be_k := E_{k,2}$

vBu := cspline(zu, Bu) vBd := cspline(zd, Bd) vBe := cspline(ze, Be)

z := -700 .. 700

Bu(z) := interp(vBu, zu, Bu, z) Bd(z) := interp(vBd, zd, Bd, z) Be(z) := interp(vBe, ze, Be, z)

z := -700 .. 700

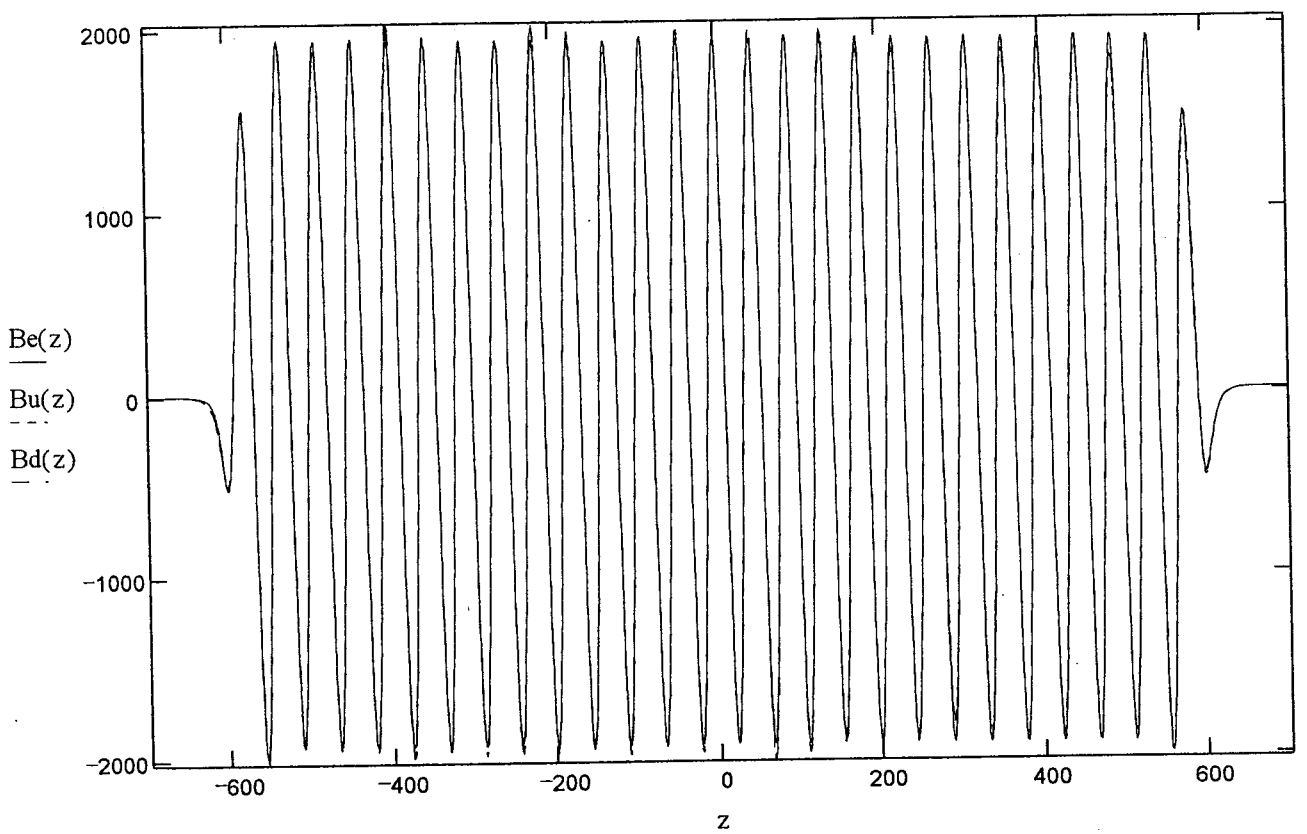

Fig. 13

$$Bau(s) := \frac{1}{44.44} \cdot \int_{s-22.22}^{s+22.22} Bu(y)\,dy \qquad Bad(s) := \frac{1}{44.44} \cdot \int_{s-22.22}^{s+22.22} Bd(y)\,dy$$

$$Bae(s) := \frac{1}{44.44} \cdot \int_{s-22.22}^{s+22.22} Be(y)\,dy$$

$i := 1 .. 1355$

$bu_i := Bau(i - 678) \qquad bd_i := Bad(i - 678) \qquad be_i := Bae(i - 678)$

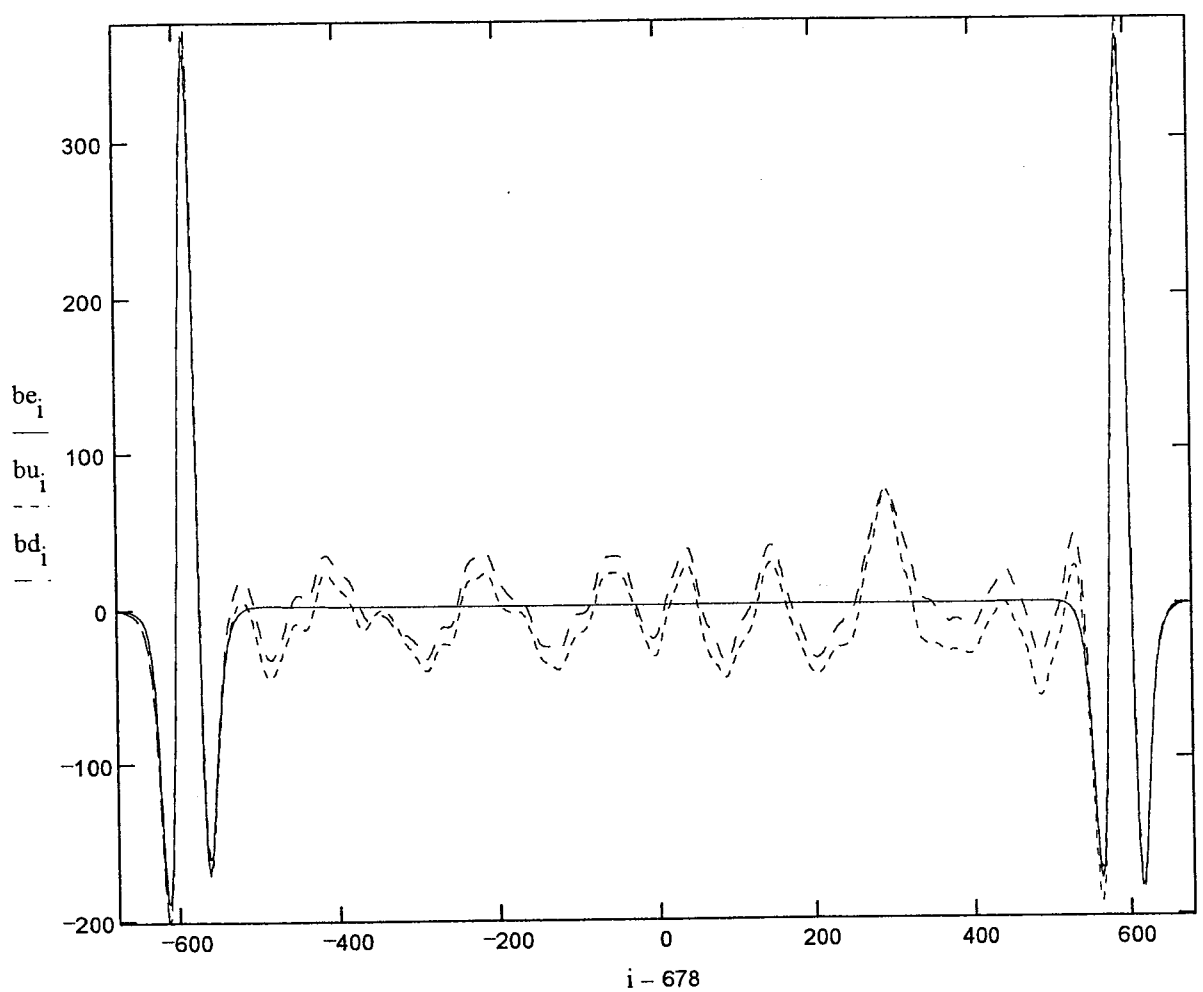

Fig. 14

Fig. 15

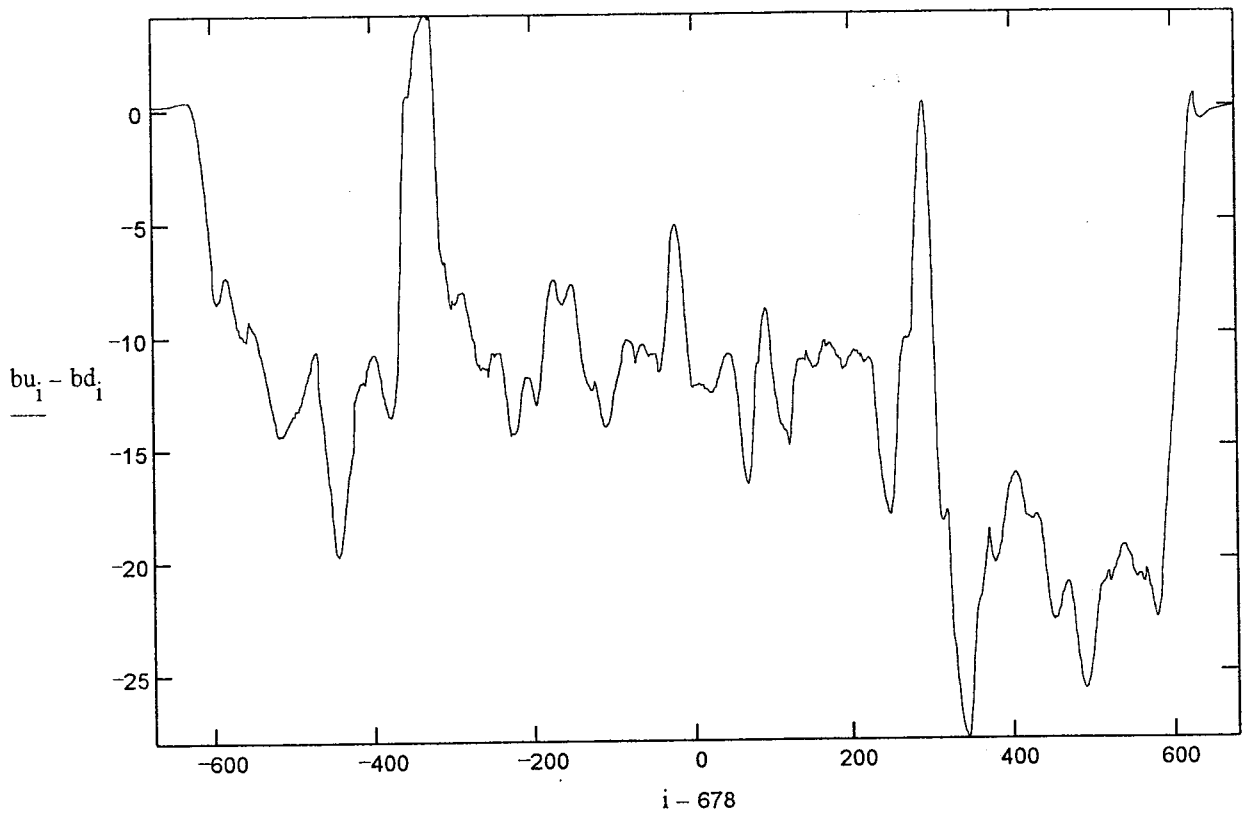

$L := 1012 \qquad N := 1278$

$$K := \frac{1.602 \cdot 10^{-19}}{9.1 \cdot 10^{-31} \cdot 3.73} \qquad K = 1 \cdot K \qquad V0 := 2.88 \cdot 10^{8}$$

$$\frac{\text{mean}(bu - bd)}{0.4} = -29.604 \qquad dB := \left[\sum_{k=L}^{N} \left(bu_k - bd_k \right) \right] \cdot \frac{1}{N - L + 1}$$

$i := 1 .. 1401$

$Bve_i := Be(i - 701) \qquad Bvu_i := Bu(i - 701) \qquad Bvd_i := Bd(i - 701) \qquad dB = -20.883 \qquad \frac{dB}{0.4} = -52.208$

$$Ve_i := \frac{K}{10^7} \cdot \sum_{j=1}^{i} Bve_j \qquad Vu_i := \frac{K}{10^7} \cdot \sum_{j=1}^{i} Bvu_j \qquad Vd_i := \frac{K}{10^7} \cdot \sum_{j=1}^{i} Bvd_j \qquad \frac{m}{sec}$$

$$Xe_i := \frac{10^{-3}}{V0} \cdot \sum_{j=1}^{i} Ve_j \qquad Xu_i := \frac{10^{-3}}{V0} \cdot \sum_{j=1}^{i} Vu_j \qquad Xd_i := \frac{10^{-3}}{V0} \cdot \sum_{j=1}^{i} Vd_j \qquad m$$

$$\left[\frac{K}{V} \right] = \frac{1}{\text{Tesla} - m}$$

Fig. 16

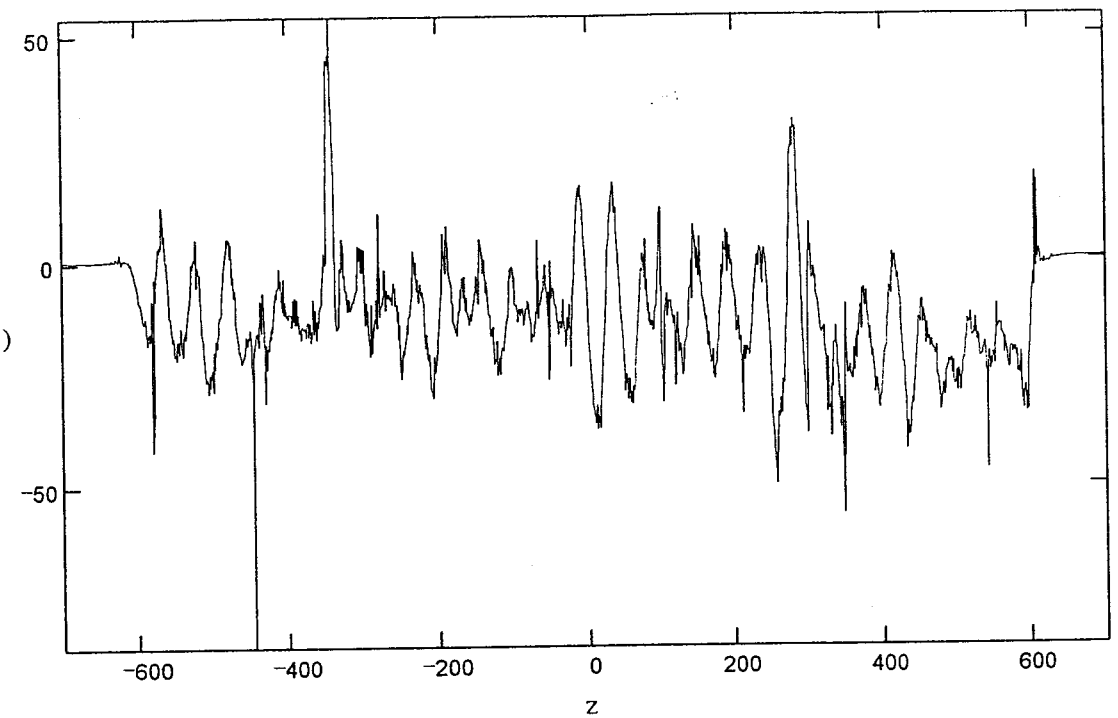
50
0
−50
Bu(z) − Bd(z)
−600
−400
−200
0
200
400
600
z

Fig. 17

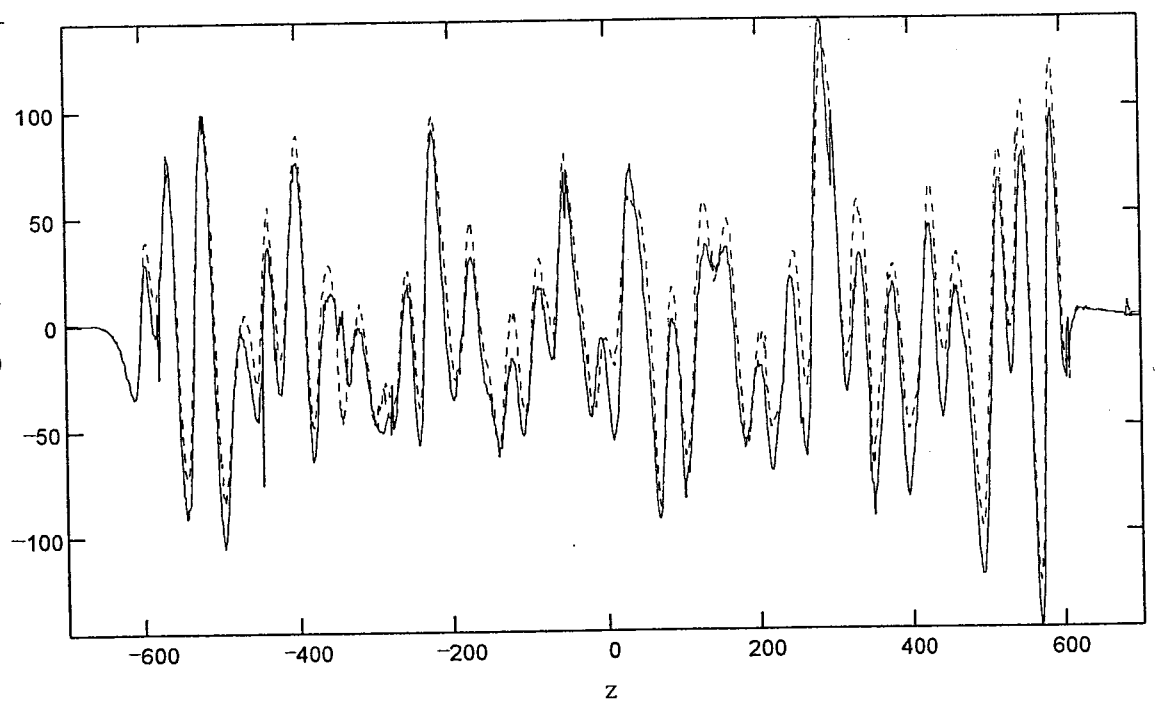
100
50
0
−50
−100
Bu(z) − Be(z)
Bd(z) − Be(z)
−600
−400
−200
0
200
400
600
z

A possible explanation is that in the back measurements the measurement axes displacement δ was larger than in the front measurements because of mechanical reasons.

The difference $\Delta B(z)$ can also be calculated directly from $\Delta B = B^{up}(z) - B^{d}(z)$ (instead of the averaged values). This however will be sensitive to sinusoidal mismatch. Fig. 16 shows this curve (compare to Fig. 15). One can see indeed a trace of the wiggler sinus (26 periods), which clutters the information on $\Delta B(z)$, which can be seen better in Fig. 15.

In Fig. 17 we also show $B_u(z)$-$B_e(z)$ and $B_d(z)$-$B_e(z)$. These should have resulted the slow functions $B^{def}(z)+B^{grad}(z)$, but again this data is cluttered by a sinusoidal modulation. Possibly smoother curves can be obtained by readjustment of the elop magnetic field by a factor that matches better the measured data. This should result in curves similar to Fig. 14 (in the inner wiggler region).

11. Determination of the magnetic axis

We now proceed to calculate the "double integral displacement function"

$$\bar{X}(z) = \frac{K}{V_0}\int_{z_i}^{z}\int_{z_i}^{z'} B(z'')dz''dz'$$

where $K = \frac{|e|}{\gamma m} = 4.72 \cdot 10^{10} \frac{1}{\text{Tesla} - sec}$

$V_0 = 2.88 \times 10^8$ m/sec $(\gamma = 3.73)$

To speed up the integration process we requantized the splined curves B_u, B_d, B_e (up, down, el-op) with 1 mm steps in the region -700 mm < z < 700 mm.
The three curves $\bar{X}_e$, $\bar{X}_u$, $\bar{X}_d$ are shown in Fig. 17a.- Fig. 17b shows seperately only $\bar{X}_e$, $\bar{X}_u$ in an enlarged scale.
A sharp trajectory deviation is observed at z ≅ 300 mm (around the "seam" location).

Because of the linearity of the integrals

$$\bar{X}(z) = \bar{X}_{id}(z) + \bar{X}_{def}(z) + \bar{X}_{grad}(z)$$

We can calculate $\bar{X}_{grad}(z)$ as a linear function of two parameters, A and B:

$$B_{grad}(z) = \begin{cases} A\frac{z+600.75}{1201.5} + B & -600.75 < z < 600.75 \\ 0 & 0 \text{ therewise} \end{cases}$$

Consequently

Fig. 17a

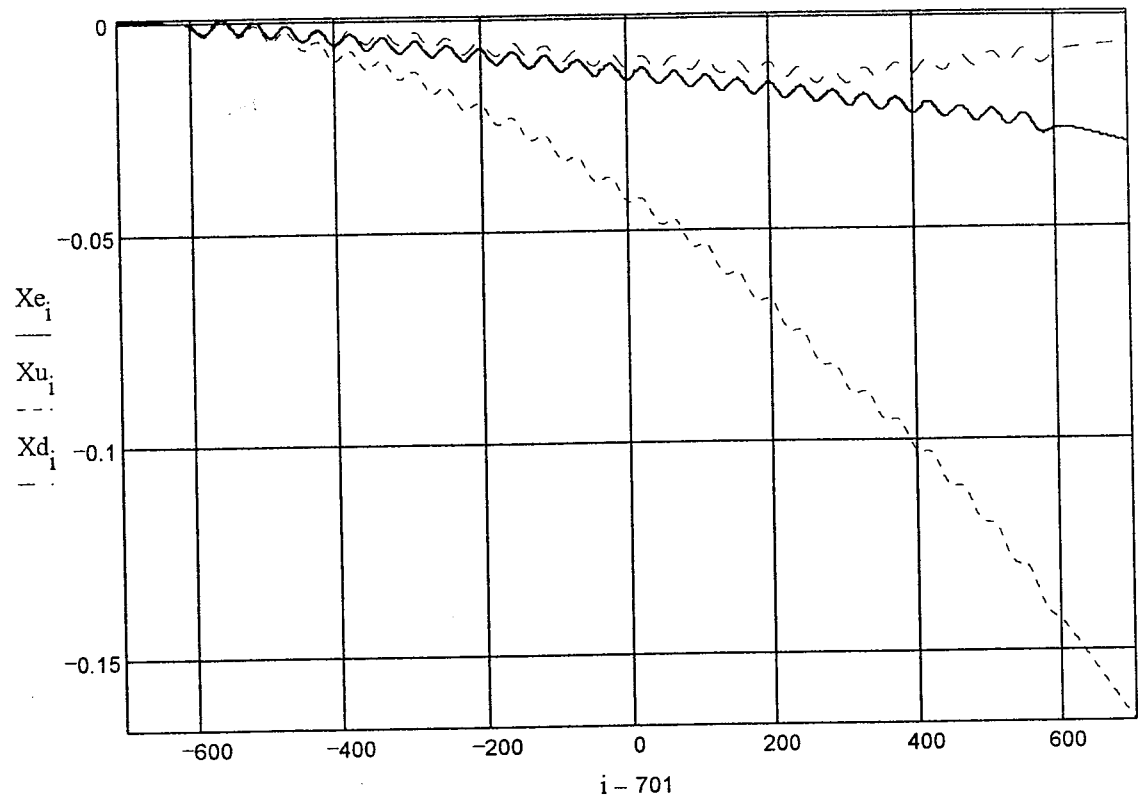

Fig. 17b

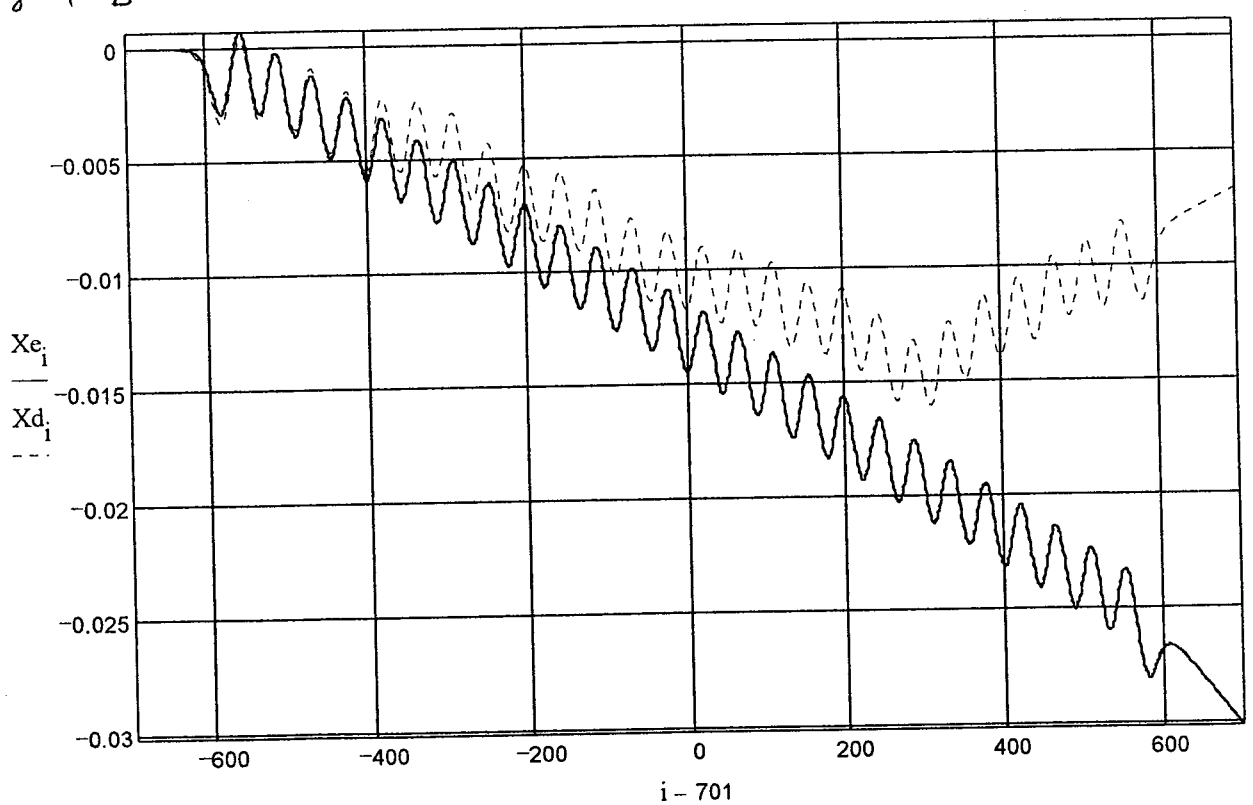

$$\overline{X}_{grad}(z) = \frac{K}{v_0}\begin{cases} 0 & z < -600.75 \\ \frac{1}{6}\cdot\frac{(z+600.75)^3}{1201.5}\cdot A + \frac{1}{2}(z+600.75)^2 B & -600.75 < z < 600.75 \\ \frac{1201.5^2}{6}A + \frac{1201.5^2}{2}B + 1201.5(z-600.75)(0.5A+B) & z > 600.75 \end{cases}$$

Clearly $\overline{X}_{grad}(z)$ is responsible for the big curved deviations of the $\overline{X}_{up}$ and $\overline{X}_{down}$ curves off the straight line behavior (after periodic averaging) of $\overline{X}_e$. Because of the defects the definition of the magnetic axis (determined by choice of A and B) is somewhat arbitrary. We decide to determine it by matching $\overline{X}(z) - \overline{X}_{grad}(z)$ to $\overline{X}_{el}(z)$ at two remote points inside the wiggler: z_a and z_b.

$$\overline{X}_{grad}(z_a; A, B) = \overline{X}(z_a) - \overline{X}_{ed}(z_a)$$
$$\overline{X}_{grad}(z_b; A, B) = \overline{X}(z_b) - \overline{X}_{el}(z_b)$$

This forms two linear equations with two unknown variables A,B, which is readily solved separately for the up and down data.
We initially chose
z_a = -499.95 mm
z_b = 211.09 mm
as the matching points. These points are both in the "front" measurement region, are spaced an integral number of periods, and correspond to nulls of the cosine function. The solution of the equation is then:

A_{up} = -6.440 Gs B_{up} = -7.971 Gs
A_{down} = -9.272 Gs B_{down} = 2.707 Gs

The function $B^{up}_{grad}(z), B^{d}_{grad}(z)$ are drawn in Fig. 18 . Note that $B^{up}_{grad}(z) < 0$ and $B^{d}_{grad}(z) > 0$ as expected

$$B^{up}_{grad}(-600.75) = B = -7.971\text{Gs}$$
$$B^{up}_{grad}(600.75) = B + A = -14.411\text{Gs}$$
$$B^{d}_{grad}(-600.75) = B = 2.707\text{Gs}$$
$$B^{d}_{grad}(600.75) = B + A = -6.565\text{Gs}$$

Through $A_{up} \neq A_{down}$, their difference is small enough to keep the field difference between the two measurement axes nearly constant.

$\Delta B = B^{up}_{grad} - B^{down}_{grad}$ = -(10.678 to 7.846) Gs along the wiggler. Compare to B_{av} = -10.9 Gs determined for the front data from Fig. 15).

left side of the wiggler

$$\int_{-600.75}^{211.09}\int_{-600.75}^{x}\left(A\cdot\frac{z+600.75}{1201.5}+B\right)\cdot 1.639\cdot 10^{-5}\,dz\,dx \qquad \frac{K}{V0\cdot 10^{7}}=1.639\cdot 10^{-5}$$

$2.32855\cdot 10^{-3}\cdot A + 8.3266\cdot 10^{-2}\cdot B$ **z=-499.95**

$1.2165\cdot A + 5.4012\cdot B$ **z=211.09**

$$M := \begin{pmatrix} 2.32855\cdot 10^{-3} & 8.3266\cdot 10^{-2} \\ 1.2165 & 5.4012 \end{pmatrix}$$

$D_1 := (Xu_{201} - Xe_{201})\cdot 1000$ **z=-499.95 i=201**

$D_2 := (Xu_{912} - Xe_{912})\cdot 1000$ **z=211.09 i=912**

$$M^{-1}\cdot D = \begin{pmatrix} -6.44 \\ -7.971 \end{pmatrix} \qquad Cu := M^{-1}\cdot D \qquad Cu = \begin{pmatrix} -6.44 \\ -7.971 \end{pmatrix} \begin{matrix} A \\ B \end{matrix} \qquad D = \begin{pmatrix} -0.679 \\ -50.887 \end{pmatrix}$$

$F_1 := (Xd_{201} - Xe_{201})\cdot 1000$ **z=-499.95 i=201**

$F_2 := (Xd_{912} - Xe_{912})\cdot 1000$ **z=211.09 i=912**

$$M^{-1}\cdot F = \begin{pmatrix} -9.272 \\ 2.707 \end{pmatrix} \qquad Cd := M^{-1}\cdot F \qquad Cd = \begin{pmatrix} -9.272 \\ 2.707 \end{pmatrix} \begin{matrix} A \\ B \end{matrix} \qquad F = \begin{pmatrix} 0.204 \\ 3.341 \end{pmatrix}$$

$$Blmu(z) := if\left(|z|>600.75, 0, Cu_1\cdot\frac{z+600.75}{1201.5}+Cu_2\right) \qquad Blmd(z) := if\left(|z|>600.75, 0, Cd_1\cdot\frac{z+600.75}{1201.5}+Cd_2\right)$$

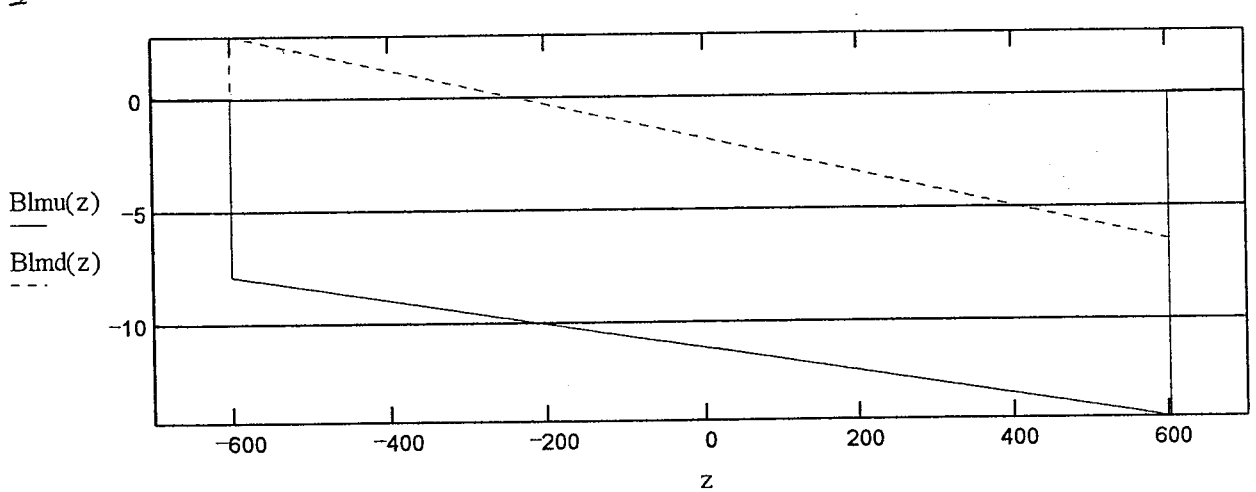

fig. 18

$Zt := 700$ $i := 1..1401$ **Zt is the point where the sets are merged**

$Xlmu(z) := if(z<Zt, Gcu(z), Hcu(z))$ $Xlmd(z) := if(z<Zt, Gcd(z), Hcd(z))$

$$Gvu_i := \frac{Xlmu(i-701)}{1000} \qquad Gvd_i := \frac{Xlmd(i-701)}{1000}$$

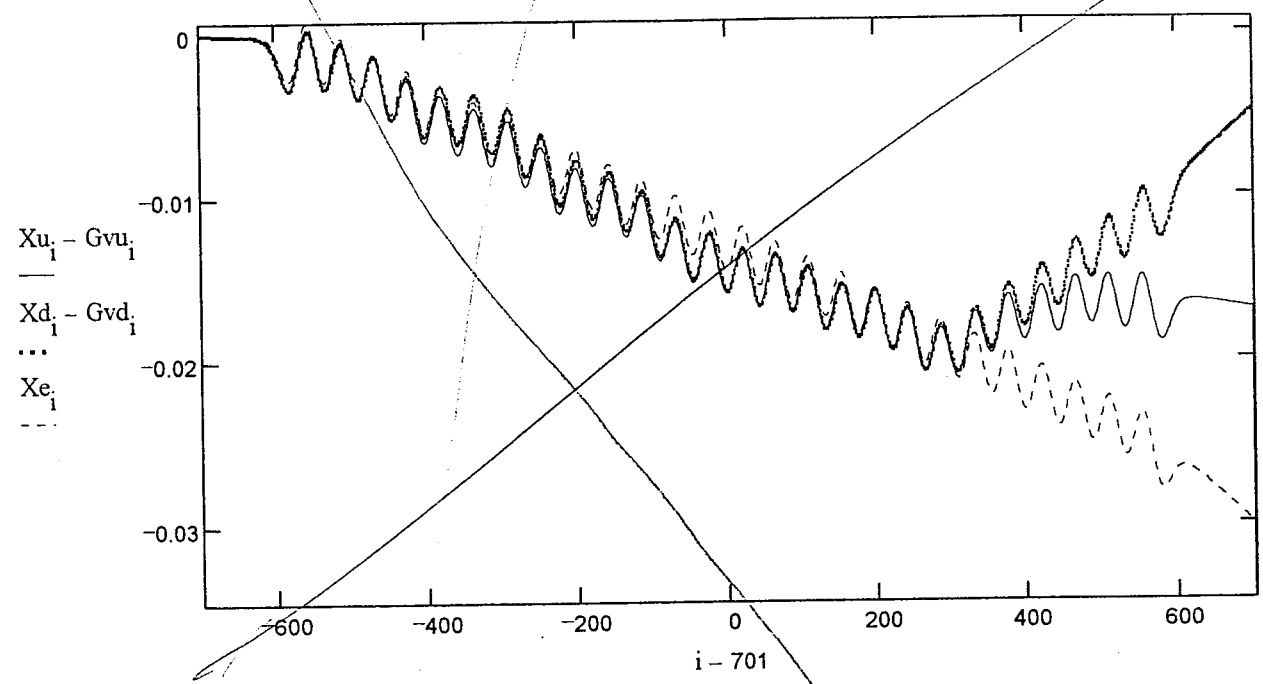

$Xu_{201} - Gvu_{201} = -0.0023425$ $Xu_{912} - Gvu_{912} = -0.01776$

$Xd_{201} - Gvd_{201} = -0.0023417$ $Xd_{912} - Gvd_{912} = -0.017747$

$Xe_{201} = -0.0023419$ $Xe_{912} = -0.017748$

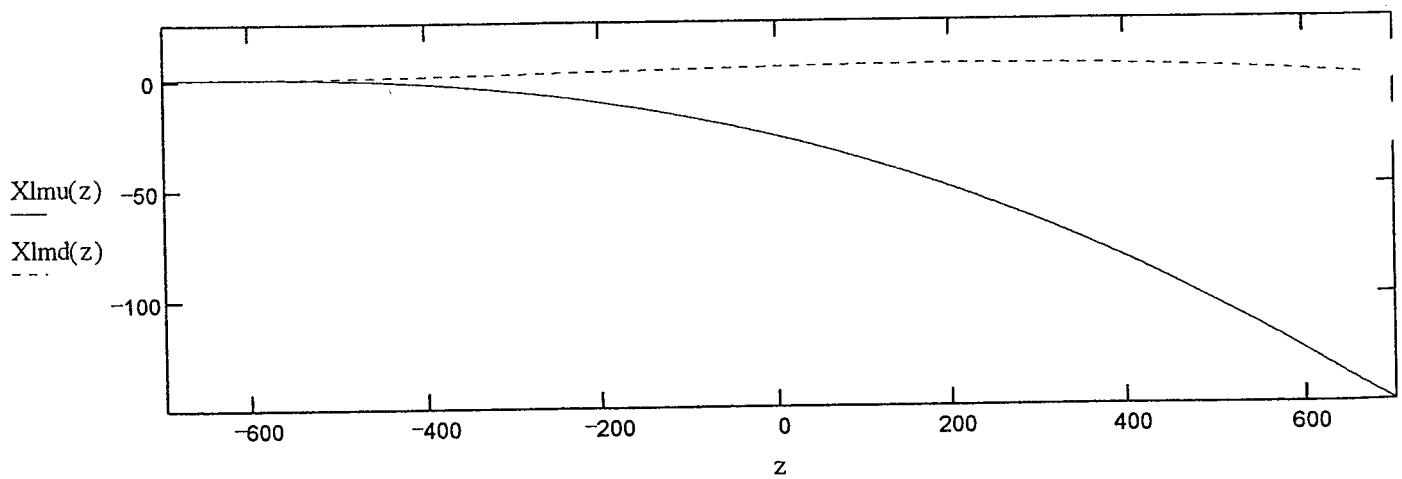

Fig 19

Fig. 20

$Gcu(z) := if(z<-600.75, 0, if(z<600.75, Gu(z), gu(z))\ Gcd(z) := if(z<-600.75, 0, if(z<600.75, Gd(z), gd(z)))$

$i := 1..1401$

$$Gu_i := \frac{Gcu(i-701)}{1000} \qquad Gd_i := \frac{Gcd(i-701)}{1000}$$

Fig. 20

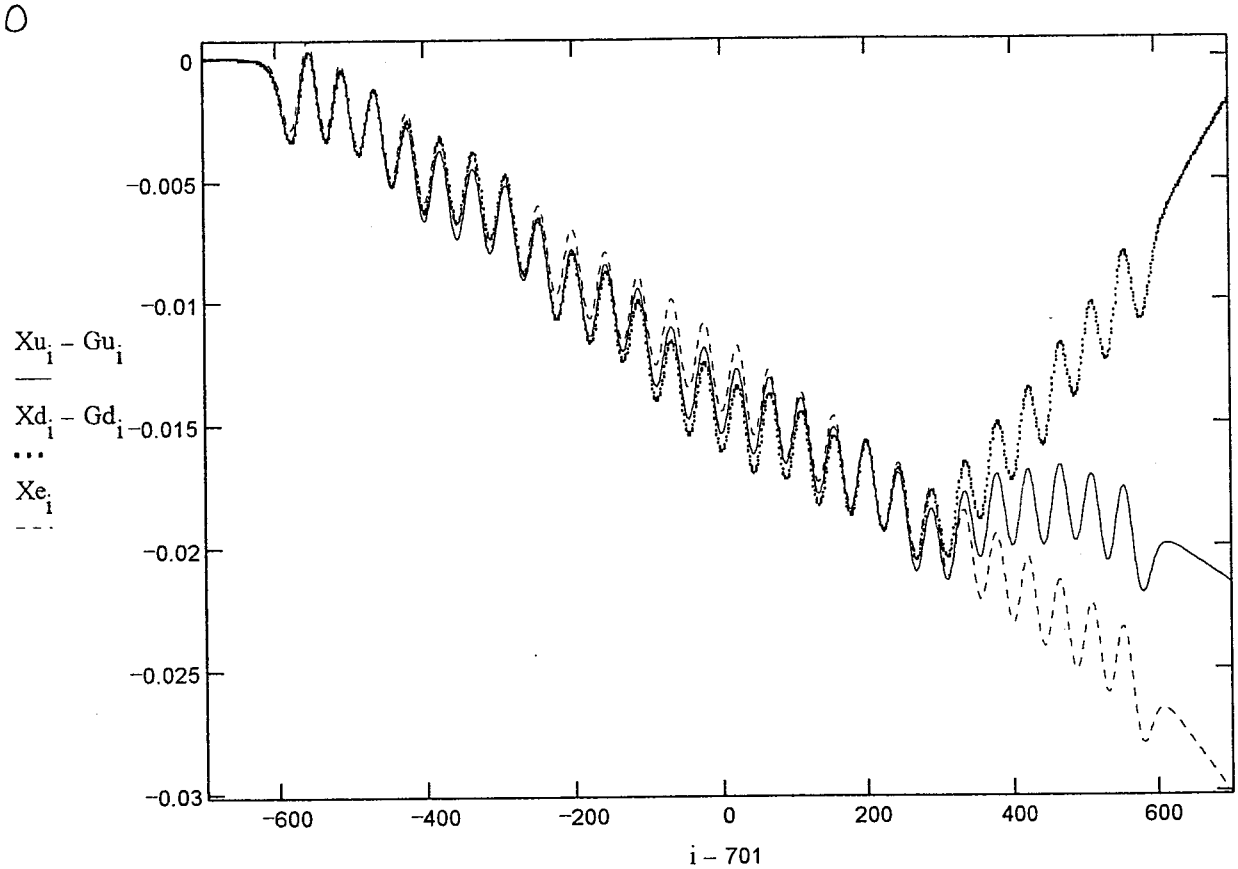

$Xu_{201} - Gu_{201} = -0.0023425$

$Xd_{201} - Gd_{201} = -0.0023417$

$Xe_{201} = -0.0023419$

$Xu_{912} - Gu_{912} = -0.01776$

$Xd_{912} - Gd_{912} = -0.017748$

$Xe_{912} = -0.017748$

$$Guo(z) := \int_{-700}^{z} \int_{-700}^{x} 1.639 \cdot 10^{-5} \cdot Blmd(s)\, ds\, dx$$

$i := 1..10$

We now can draw the displacement function due to the gradient field $\overline{X}_{grad}(z)$ for the "up" and "down" measurements (Fig. 19), and by subtracting them from $\overline{X}(z)$:

$$\overline{X}_{axis}(z) = \overline{X}(z) - \overline{X}_{grad}(z)$$

We obtain essentially the "double integral trajectory" on axis.

This is shown in Fig. 20 for $\overline{X}^{up}_{axis}$, $\overline{X}^{d}_{axis}$ together with $\overline{X}_e$ for comparison. The three curves cross at the two chosen matching points. One can note that the "entrance angle" is correct and that along the wiggler the deviation of the trajectory from the ideal curve is maximum 3 mm (in the -X direction, taking place near the center of the wiggler).

The big deflection near z = 300 mm takes place for both the up and down curves and will be explained later.

12. Improved determination of the magnetic axis

The big deflection of the trajectories cannot be ignored, and seems to be correlated to the jump in $\Delta B_{grad}(z)$ near the "seam" point. We considered the possibility that it reflects a real physical problem (possibly due to change in magnet strength of the periods added when the wiggler was evaluated). This explanation should still be checked out but our preferred explanation is that the "back" measurements took place along a different axis than the "front" measurements because of the available freedom transverse of movement left for the probe inside its rail and due to moments applied by the long screw on the block (see discussion in sect. 7).

Based on this assumption we go ahead to determine separately $A^{up,d}$ and $B^{up,d}$ for the "front" and "back" measurements. The matching points were taken this time to be

Z_a = -510.36 mm	Z_b = 334 mm	for the "front" data
Z_a = 334 mm	Z_b = 556.2 mm	for the "back" data

where z = 334 mm is the "seam" point. These points are spaced by a multiple of a period but are not "zero" filed points (inevitably). We hope that this does not introduce a significant error. The result of $B_{grad}(z)$ is shown in Fig. 21 for the up and down axes. Also we show in Fig. 22 the measurement axes and mechanical axis position $X_u(z)$, $X_d(z)$, $X_{mech}(z)$ related to the magnetic axis X=0. In doing this, we assume (based on previous measurement - see report of June 15, 1997) that α = -25 Gs/mm and that the mechanical axis is the average of the two measurement axes, thus

$$X_{up}(z) = \frac{B^{up}_{grad}(z)}{\alpha}$$

$$X_{d}(z) = \frac{B^{d}_{grad}(z)}{\alpha}$$

$$X_{mech,ax}(z) = \frac{1}{2} \cdot \frac{B^{up}_{grad}(z) + B^{d}_{grad}(z)}{\alpha}$$

$Z0 := 334$

$Baxu(z) := if(z<Z0, Blmu(z), Brmu(z))$

$Baxu(Z0 + 1) - Baxu(Z0 - 1) = -1.327$

$Baxd(z) := if(z<Z0, Blmd(z), Brmd(z))$

$Baxd(Z0 + 1) - Baxd(Z0 - 1) = 2.082$

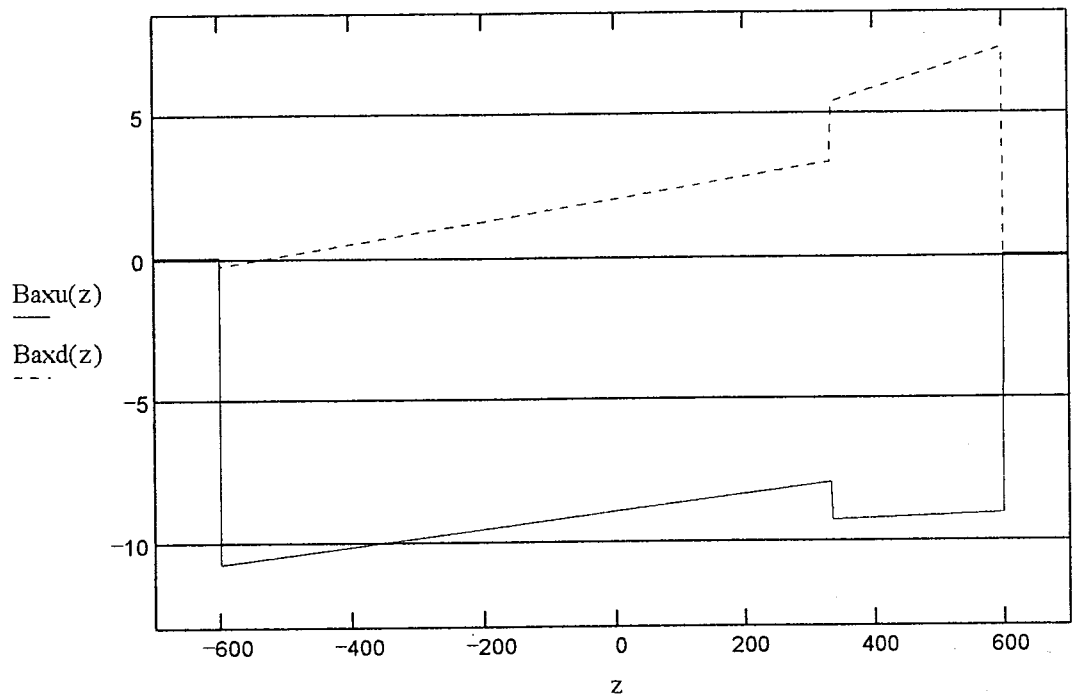

Fig. 21

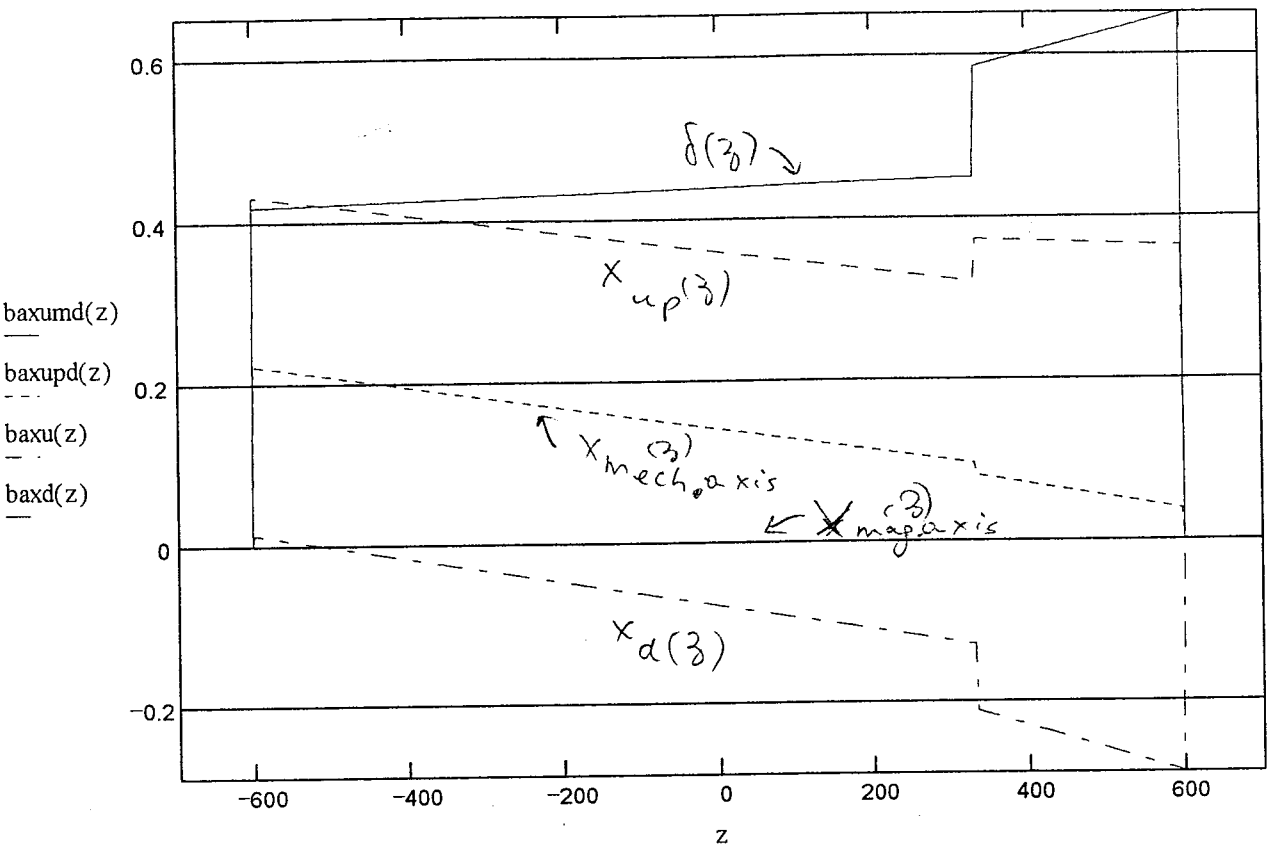
baxumd(z)
baxupd(z)
baxu(z)
baxd(z)
0.6
0.4
0.2
0
−0.2
−600
−400
−200
0
200
400
600
z
δ(3)
x_up(3)
x_mech.axis(3)
x_map.axis(3)
x_d(3)

Fig. 22

$$\delta(z) = \frac{1}{\alpha} \cdot \left[B^{up}_{grad}(z) - B^{d}_{grad}(z) \right]$$

It is quite satisfying to see that these parameters, and especially $\delta(z)$, are close to the expectation within the predicted mechanical tolerances.

Fig. 23 now shows $\overline{X}^{up}_{grad}(z)$, $\overline{X}^{d}_{grad}(z)$ and Fig. 24 shows the $\overline{X}^{up}_{axis} = \overline{X}^{up} - \overline{X}^{up}_{grad}$ and $\overline{X}^{d}_{axis} = \overline{X}^{d} - \overline{X}^{d}_{grad}$ together with $\overline{X}_{el}(z)$. The match of the three curves seems now pretty good. Fig. 25a shows an enlargement of the matching area (at the "seam" location z=334 mm). Note that the amplitude of $\overline{X}_{el}$ is significantly smaller than $\overline{X}_{up}$ and $\overline{X}_{d}$ and because the matching point is not a "zero", this could introduce some error in the axis parameter determination. It may be a good idea to try to repeat the match with another z_b.

13. Wiggler quality parameters

If we rely on Fig. 24, then the following conclusions may be made:

a. The measurement "double integral trajectory" on axis is close to the ideal el-op double integral trajectory within 2 mm displacement (Fig. 24). This is not negligible, but the gradient focusing may help to overcome this deviation.

b. The deviation of the measured data entrance and exit angles from the El-Op predictions (deduced from Fig. 24, 25b,c) are:

	from "up" data	from "down" data	from El-Op
α_{in} =	- 22 mrad	- 22 mrad	- 22 mrad
$\Delta\alpha_{in}$ =	0	0	_____
α_{out} =	- 33 mrad	- 18 mrad	- 21 mrad
$\Delta\alpha_{out}$ =	- 12 mrad	+ 3 mrad	_____

The double integral trajectory entrance and exit angles of El-Op (- 21 to - 22 mrad) correspond to a case of optimized entrance and exit magnets that assure on axis propagation of the beam into and out of the wiggler. Hence $\Delta\alpha_{out}$, $\Delta\alpha_{in}$ correspond approximately to deviations due to inaccuracies in the magnets that will need to be compensated by the entrance and exit steering coils. It is more likely that this deviations are a result of the measurement and data matching inaccuracies. In any case angles deviations - 12 mrad $< \Delta\alpha <$ 3 mrad can easily be compensated by our steering coils. No deviation is observed at the entrance ($\Delta\alpha_{in} = 0$).

It is interesting also to try to compute the defect fields on axis and draw some future operative conclusions. As in Fig. 17 we again subtract the El-Op magnetic field from the on axis magnetic field computation from the up and down measurements. In order to obtain the defects field $B^{def}(z)$:

$(B^{def})_{up} = B^{up}_{axus} - B_{el}$

$(B^{def})_{d} = B^{d}_{axis} - B_{el}$

$Zt := 334$ $i := 1..1401$ **Zt is the point where the sets are merged**

$Xlmu(z) := if(z<Zt, Gcu(z), Hcu(z))$ $Xlmd(z) := if(z<Zt, Gcd(z), Hcd(z))$

$$Gvu_i := \frac{Xlmu(i-701)}{1000} \qquad Gvd_i := \frac{Xlmd(i-701)}{1000}$$

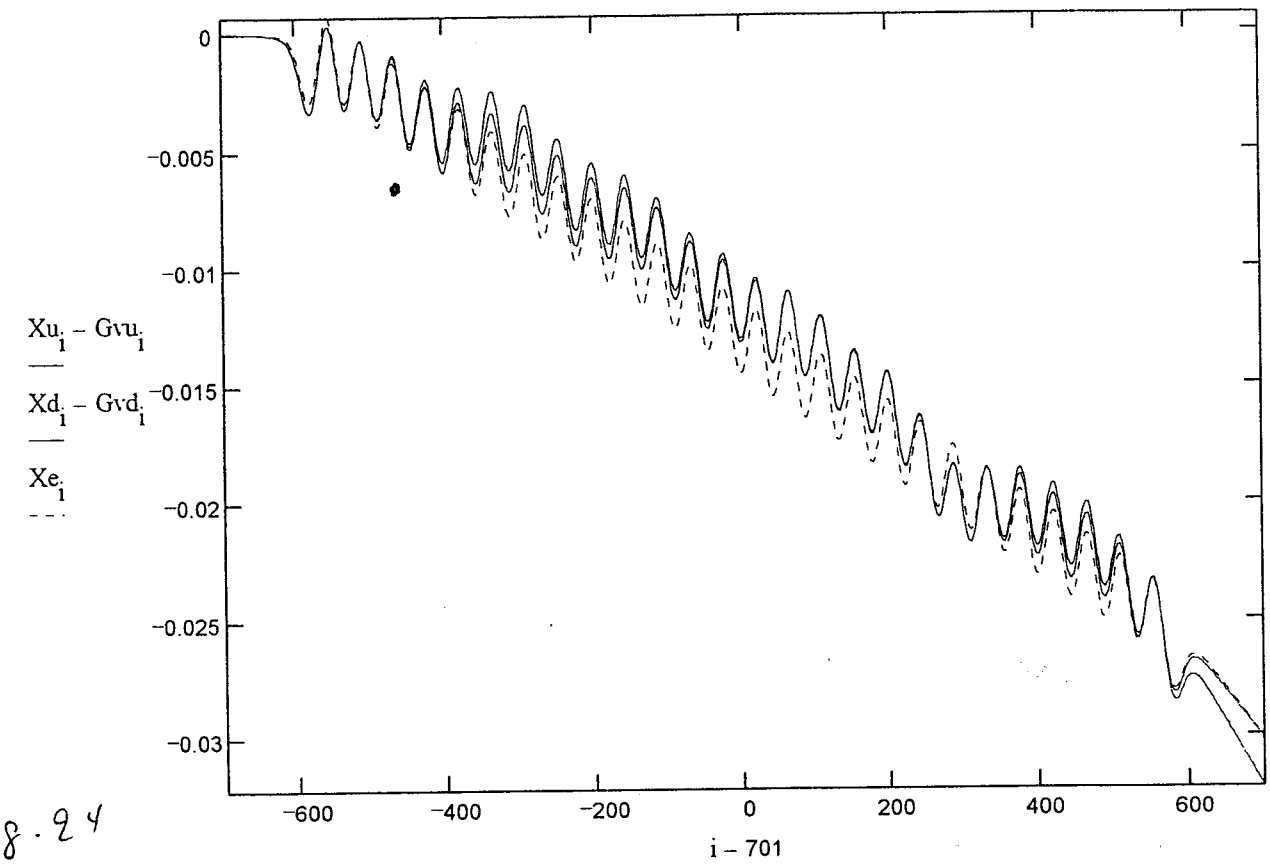

Fig. 94

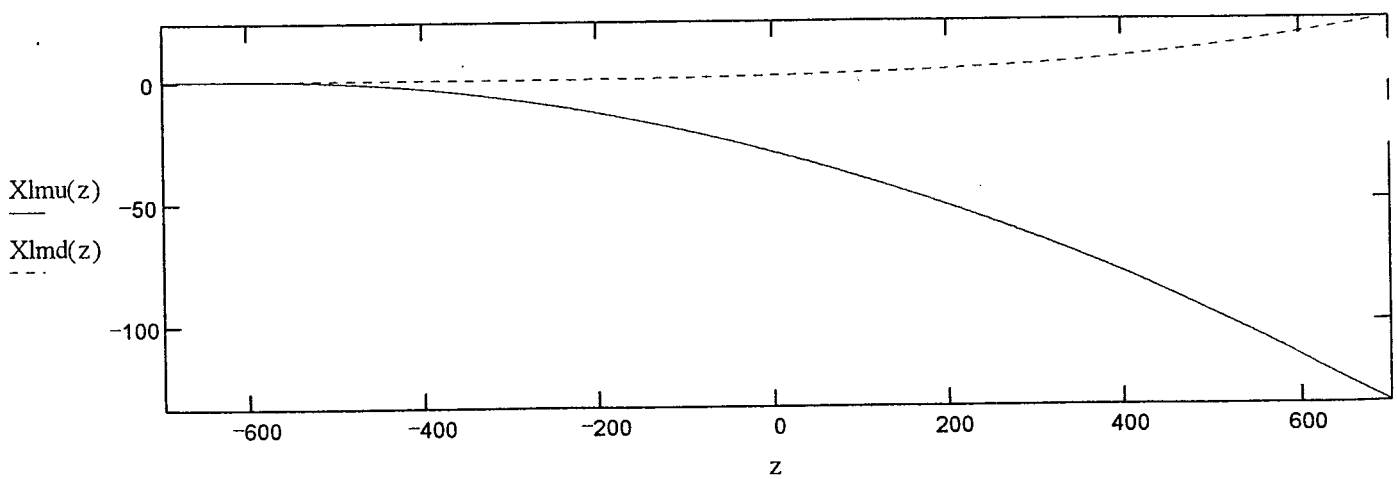

Fig. 93

$Zt := 334$ $i := 1000 .. 1080$ **Zt is the point where the sets are merged**

$Xlmu(z) := if(z<Zt, Gcu(z), Hcu(z))$ $Xlmd(z) := if(z<Zt, Gcd(z), Hcd(z))$

$$Gvu_i := \frac{Xlmu(i - 701)}{1000} \qquad Gvd_i := \frac{Xlmd(i - 701)}{1000}$$

Fig 25a

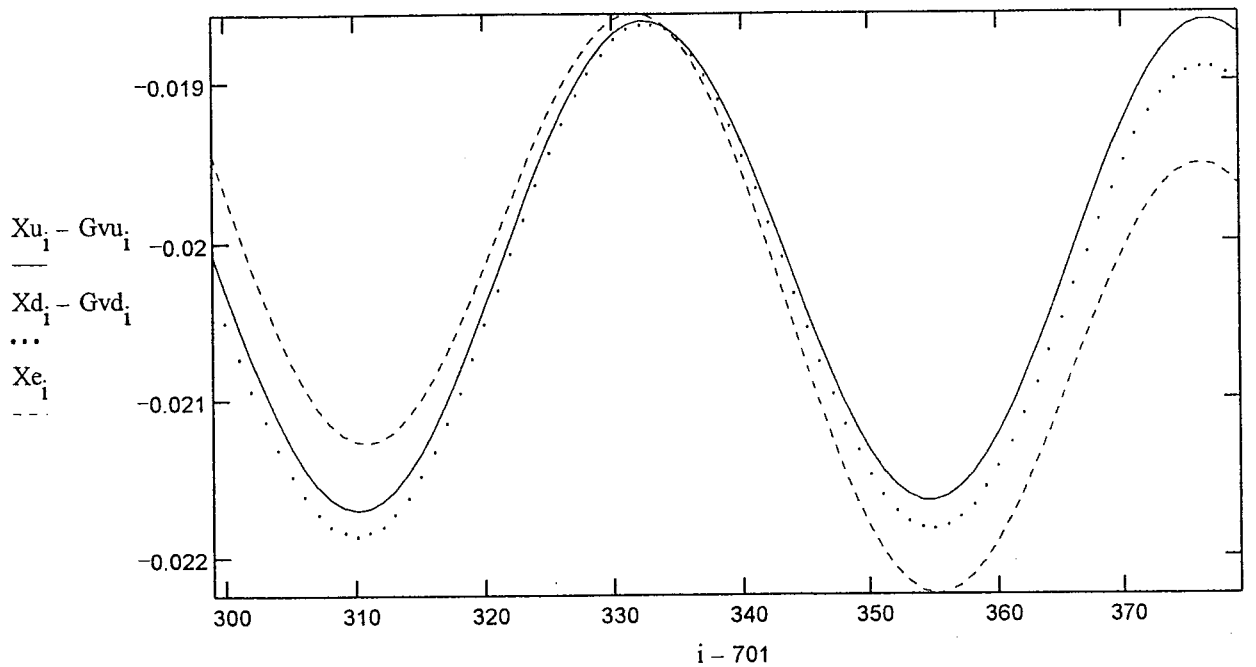

$Xu_{201} - Gvu_{201} = -0.0021322$ $Xu_{912} - Gvu_{912} = -0.016268$

$Xd_{201} - Gvd_{201} = -0.0021217$ $Xd_{912} - Gvd_{912} = -0.016977$

$Xe_{201} = -0.0023419$ $Xe_{912} = -0.017748$

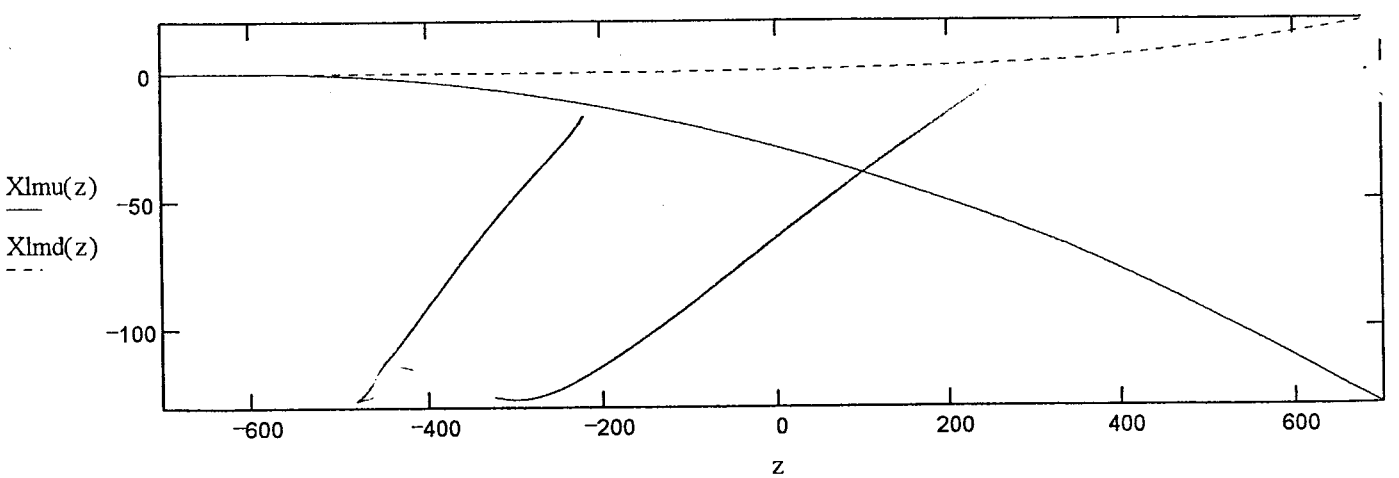

$Zt := 334$ $i := 1 .. 1401$ **Zt is the point where the sets are merged**

$Xlmu(z) := if(z<Zt, Gcu(z), Hcu(z))$ $Xlmd(z) := if(z<Zt, Gcd(z), Hcd(z))$

$Gvu_i := \frac{Xlmu(i - 701)}{1000}$ $Gvd_i := \frac{Xlmd(i - 701)}{1000}$ $i := 1 .. 150$

Fig. 25b

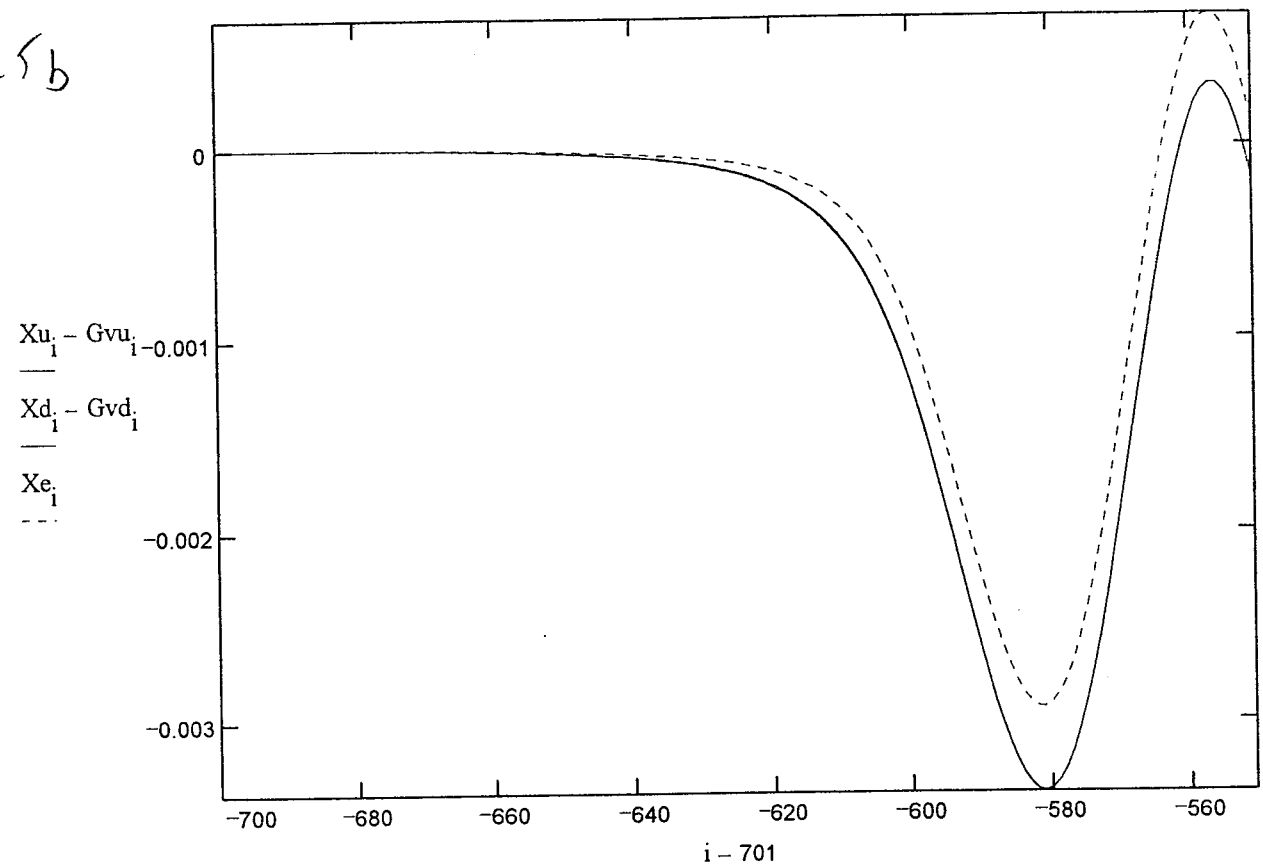

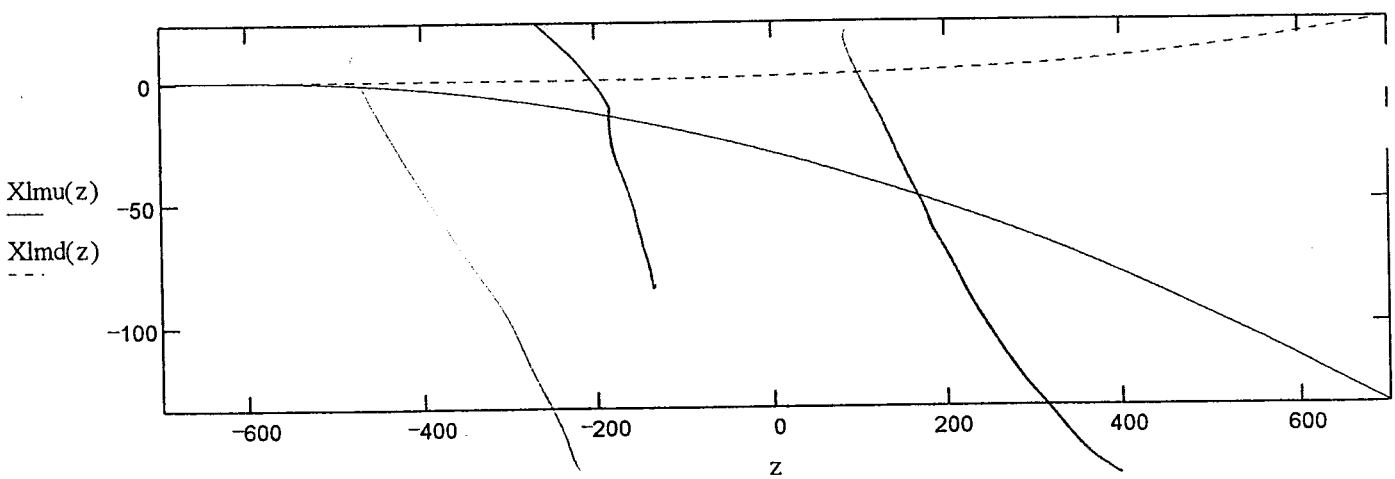

$Zt := 334$ $i := 1..1401$ **Zt is the point where the sets are merged**

$Xlmu(z) := if(z<Zt, Gcu(z), Hcu(z))$ $Xlmd(z) := if(z<Zt, Gcd(z), Hcd(z))$

$Gvu_i := \frac{Xlmu(i-701)}{1000}$ $Gvd_i := \frac{Xlmd(i-701)}{1000}$ $i := 1250..1400$

Fig. 95C

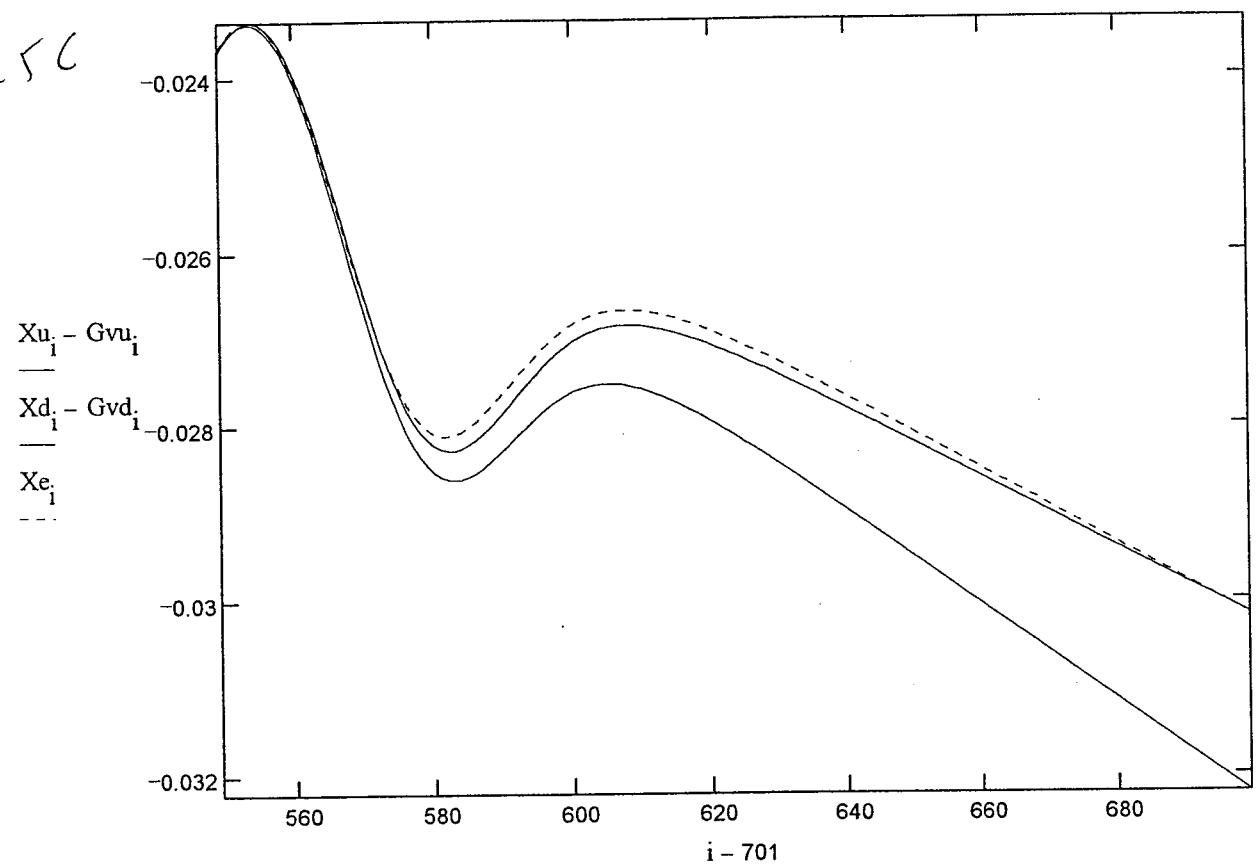

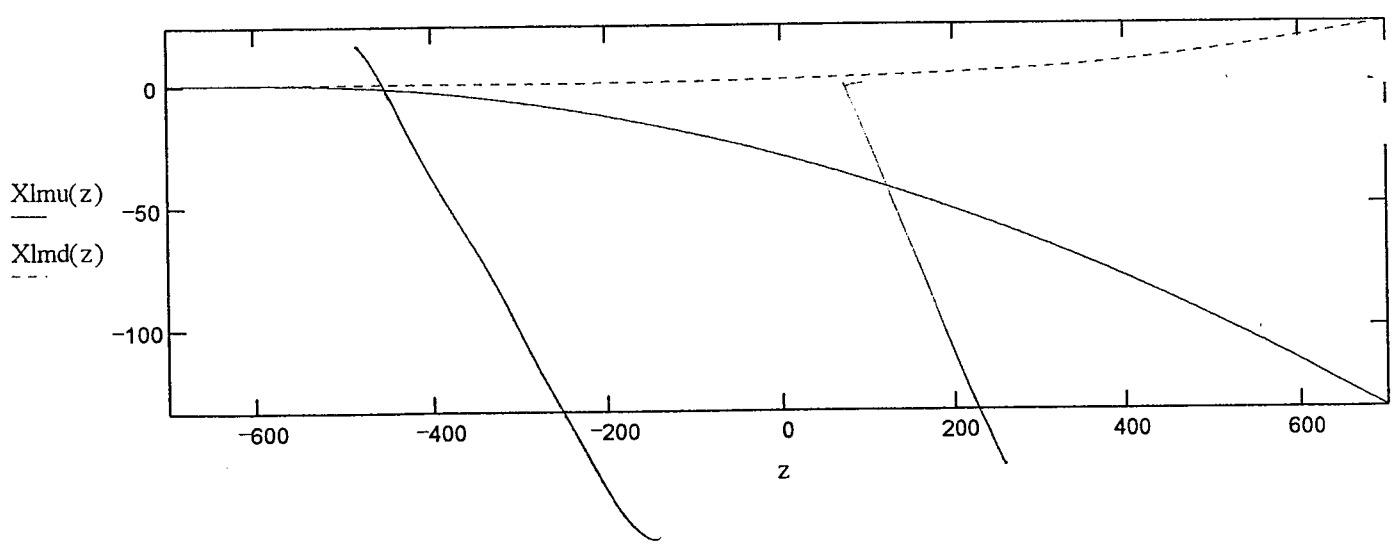

z

Fig. 27: Substruction of the up and down measurements data to obtain the gradient field

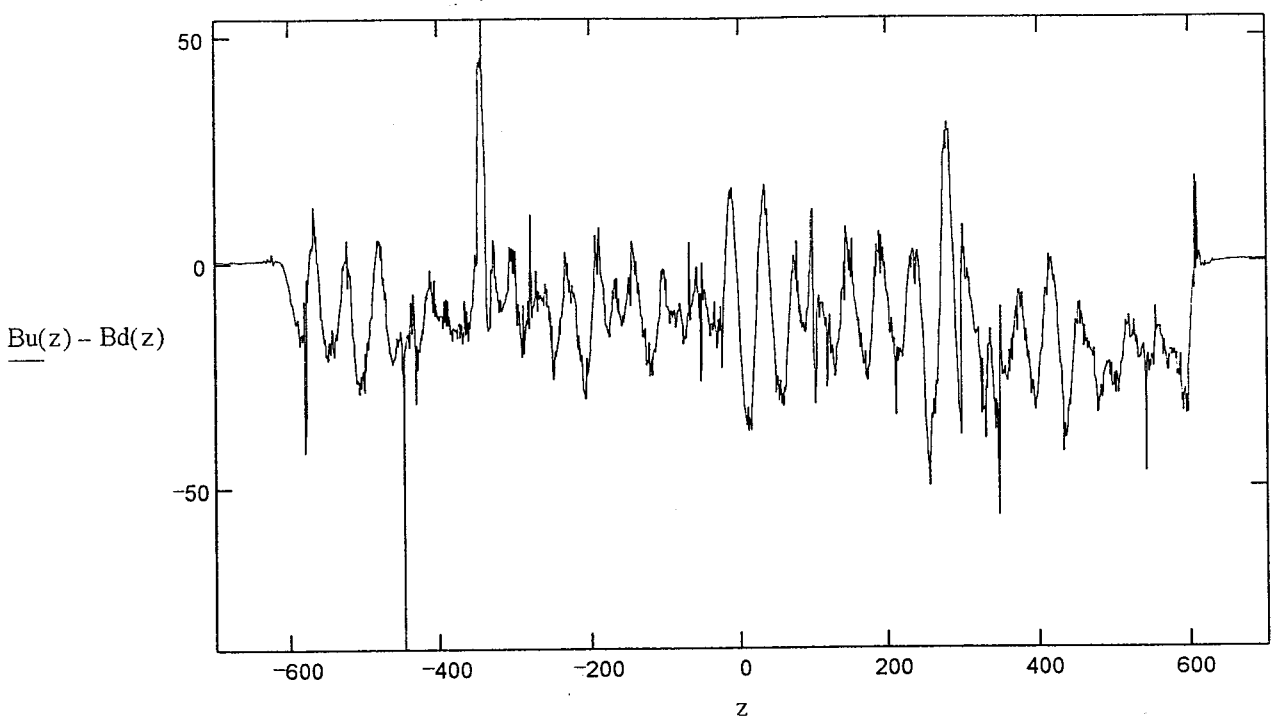

Fig. 26: Net defect field

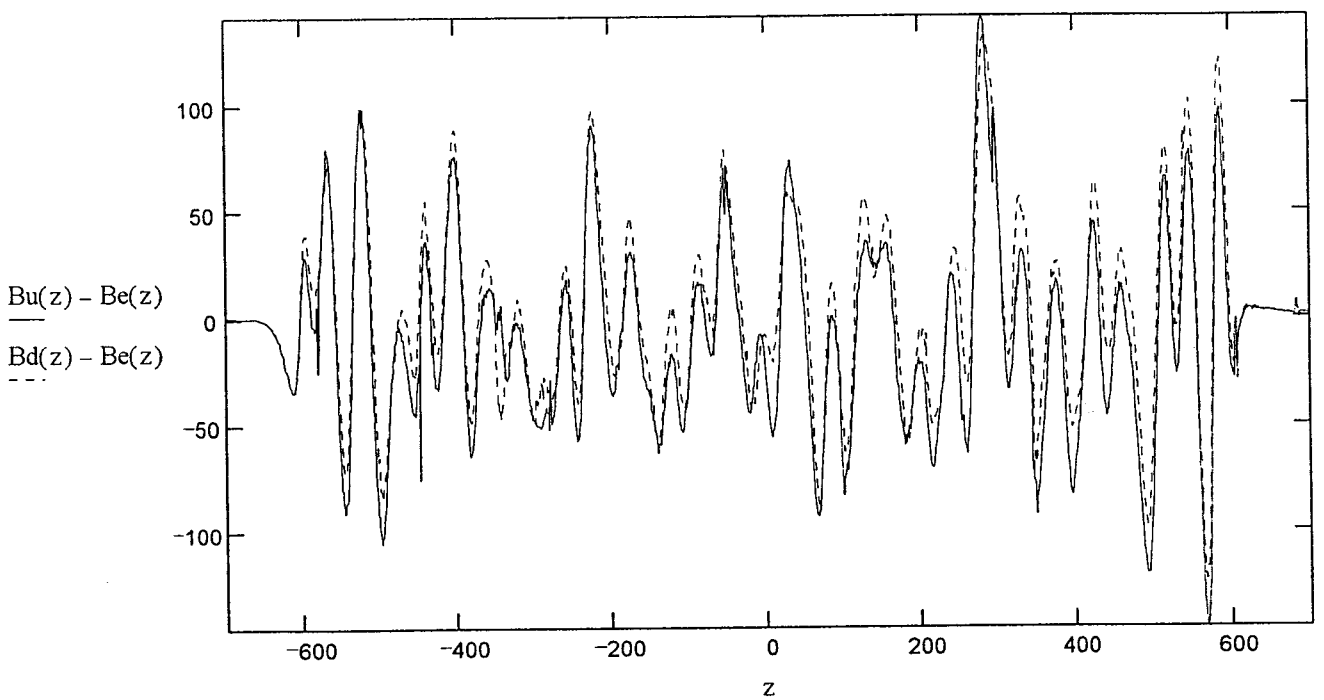

The result (Fig. 26) is heavily cluttered by periodic perturbation due to mismatch of the El-Op field amplitude and the measured data. To improve the data we tried to readjust the amplitude of the El-Op field by finding min. (B^{up} - B^{up}_{av}-kB_{el}) over a region -500 < z < +500,, but we did not succeed to get a value significantly better than k = 1. It seemed that good match in the front part of the wiggler led to bad match at the back and vice versa. This probably indicated that matching of the front and back data is not good enough, or that magnets strenght is different in the two parts of the wiggler.

The curve in Fig. 26 should represent the net defect field and the curve in Fig. 27 - $B_u(z)$ - $B_d(z)$ should represent the gradient filed. They are both badly cluttered. Fig. 26 should be compared with the averaged fields in Fig. 14 which are much smoother but may include some distortion at the defect fields. Fig. 27 should be compared with Fig. 15 that is also noisy, but more informative

It is interesting to compare defect of Fig. 26 and its "double integral function" (Fig. 28) to the field and double integral displacement computed with El-Op for the correction magnets along the wiggler (Figs. 28, 29 which were taken from report of 25.6.97). The comparison should indicate the efficiency of the correction magnets in correcting fields and displacements, and can also point to "over - correction". The difference between the curves in Fig. 26 and 28 and the difference between the curves in Fig. 27 and 29 should be the original defect field (before correction) and the trajectory deviation before the correction. Fig. 28 indicates quite balanced up and down deviations due to defects and magnet corrections - not more than 2 mm. Comparison to Fig. 29 indicates that the correction magnets improved the wiggler significantly.

14. Comparison to Pulsed Wire Experiments

Fig. 30 displays a pulsed wire measurement (proportional to a double integral function) of the wiggler, performed by J. Sokolowski on .7.97. This trajectory was found after adjusting the wire position to a situation close to wiggling along a straight line (a process analogous to our numerical search for the magnetic axis).

The comparison of Fig. 30 to Fig. 24 (note that the first and last wiggles are in the down direction, so that in both figures the +x axis is the same) reveals that they both predict (not real) initial entrance and exit angles in the -x direction (In Fig. 24 $\alpha_{in} \cong \alpha_{out} \cong$ -21 mrad, in Fig. 30 $\alpha_{in} \cong$ -13.1 mrad, $\alpha_{out} \cong$ -14 mrad).

Inside the wiggler the trajectory curves slightly in the +x direction in Fig. 24 and in the -x direction in Fig. 30. It is possible that a little better adjustment of the wire could have removed this discrepancy.

15. Conclusions

a. The wiggler seems to be now of good enough quality to put back into the tank. Steering coil capability of ± 20 mrad exactly at the entrance and exit of the wiggler should be enough to correct possible error and imperfections.

b. The correcting magnets seem to correct the original defects quite satisfactorily.

c. The measurement data can be processed better with more time given. This can be done at leisure using other programs for a test (e.g. MathLab - with the help of ~~Rouven~~ Ronen) without delaying the experimental steps.

d. For future magnetic field measurement we should prepare:

1. A new accurate Hall probe with computer interface ~~for~~ to replace our broken instrument.
2. An accurate Mechanical Movement stage that will enable automatic movement (with a stepping motor) and position reading along 1.4 m without interruption.
3. Micrometer transverse displacement adjustment of the movement axis.
4. Two axes measurements seems to be a good method. The displacement of the axes should be larger, perhaps 1 mm ($\Delta B \cong 25$ Gs), if one wants to measure the gradient accurately.

$$Xdefd_i := \frac{10}{V0} \cdot \sum_{j=1} Vdefd_j \qquad Xdefu_i := \frac{10}{V0} \cdot \sum_{j=1} Vdefu_j$$

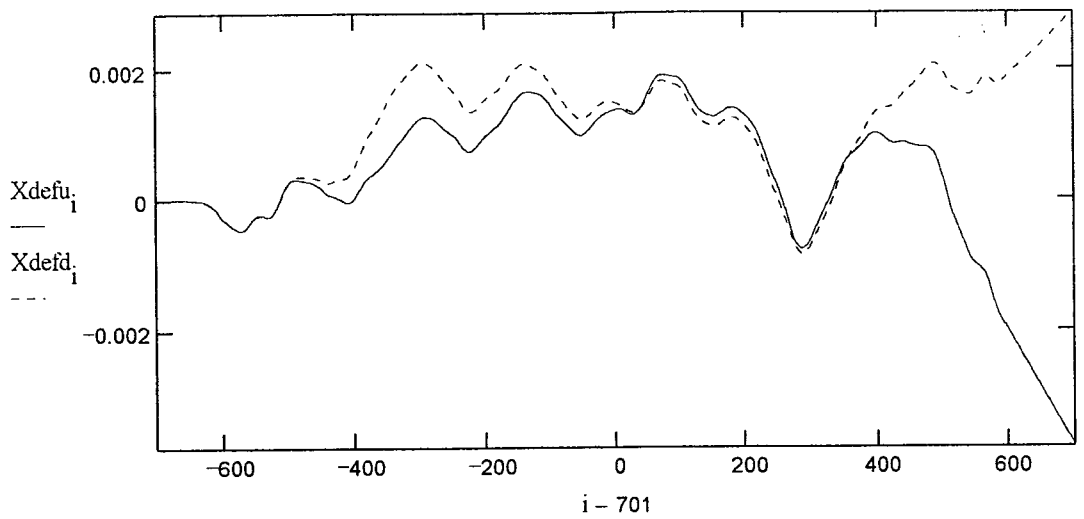

Fig. 28: Integral of integral x-displacement due to the defect magnetic field of Fig. 26.

g. 29: Magnetic field of the glued correction magnets calculated with ELOP

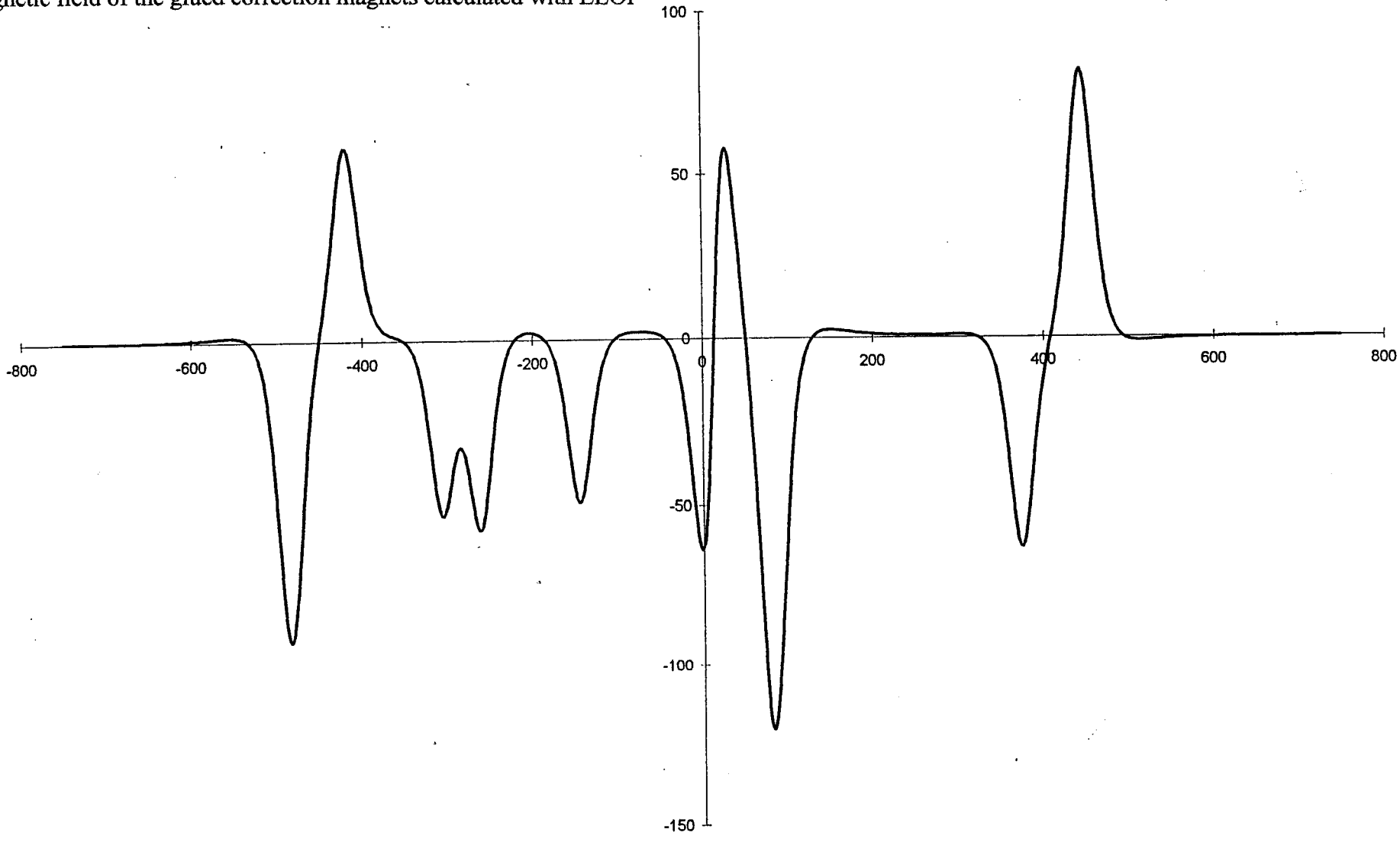

g. 30: Integral of integral x-displacement due to the magnetic field of the glued
orrection magnets calculated with ELOP (Fig. 29)

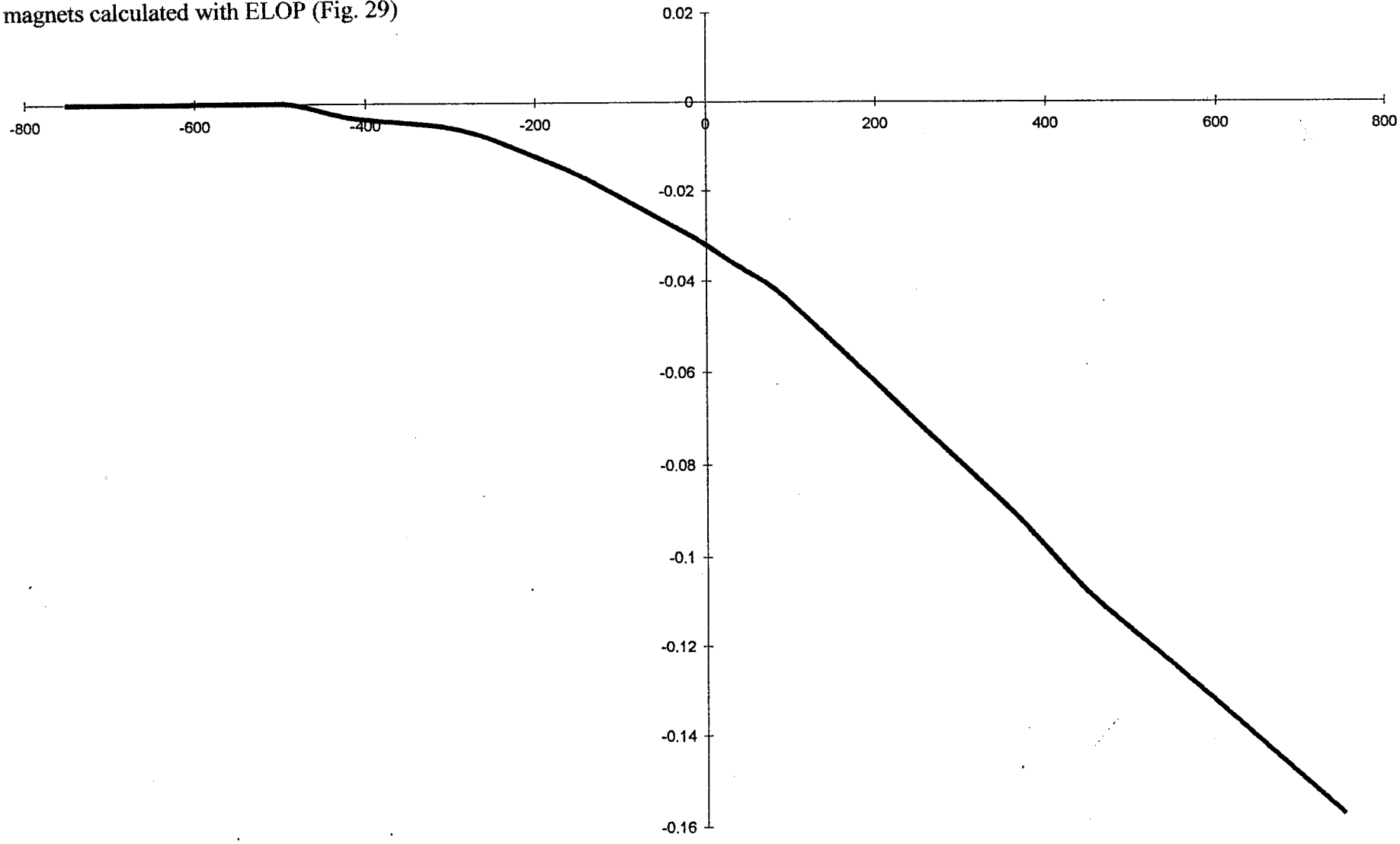

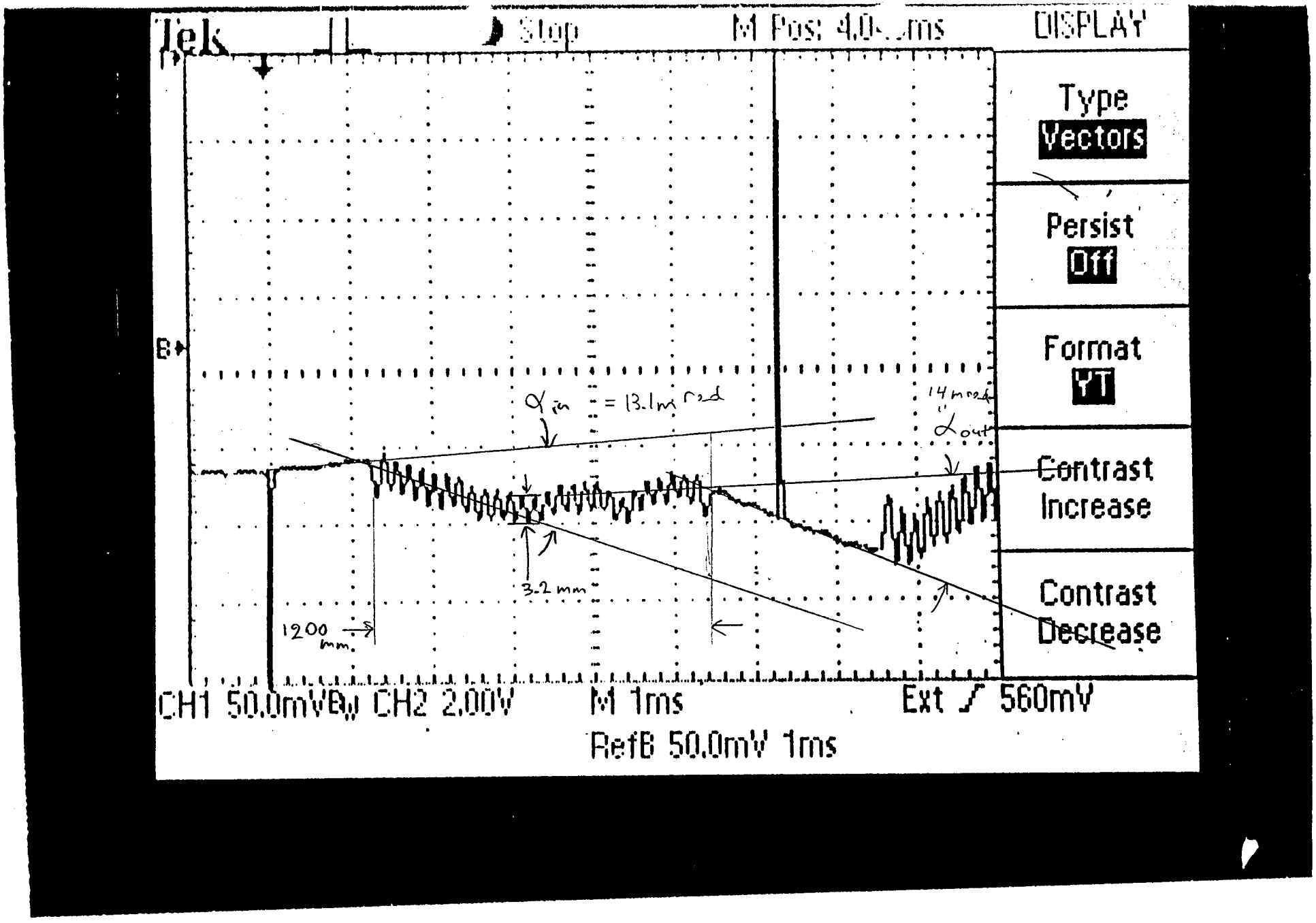

Fig. 30

$\frac{30}{70} \times \frac{3.9}{6} \cdot \frac{1}{1200} = 13.1\ m\ rad$

$\frac{27}{59} \times \frac{3.9}{1} \cdot \frac{69}{1200} = 14\ m\ rad$